AN ABSTRACT OF THE THESIS OF

REX WAI-YUEN TANG (Name) for the MASTER OF SCIENCE (Degree)

in OCEANOGRAPHY (Major) presented on April 24, 1974 (Date)

Title: GEOTHERMAL EXPLORATION BY TELLURIC CURRENTS IN THE KLAMATH FALLS AREA, OREGON

Abstract approved: Redacted for Privacy

Geothermal resources are characterized by a very low electrical resistivity of the reservoir formations. The application of electrical methods in the reconnaissance type exploration for such resources is discussed. It is concluded that the magneto-telluric method is very well suited for this purpose.

In 1971 and 1972 a reconnaissance type magneto-telluric field program was carried out in southern and eastern Oregon by the Geophysics Group at Oregon State University. In order to reduce the field effort, the magnetic data were obtained from a fixed base station at Corvallis. Only the electrical field components were measured at the various field stations. Ten stations were occupied in the Klamath Falls area, six in central and eastern Oregon and one in the Willamette Valley.

Impedance data were obtained in the .025 to 0.05 Hz frequency band of the Pc 3 micropulsations. The data were analysed on the basis

of an individual event method. Only magnetic-telluric events with a good correlation are taken into account.

The resulting apparent resistivities display some correlation with known geothermal manifestations in the region. The lowest resistivities of the order of 10 ohm-meters were recorded in the Klamath Falls region and at a station near Vale in eastern Oregon. As common in magneto-telluric work, the data display a considerable variability, irregular scattering and anisotropy.

The results are encouraging in that they appear to indicate that the magneto-telluric method is a useful reconnaissance method in the regional exploration for geothermal resources.

Geothermal Exploration by Telluric Currents in the Klamath Falls Area, Oregon

by

Rex Wai-Yuen Tang

A THESIS

submitted to

Oregon State University

in partial fulfillment of
the requirements for the
degree of

Master of Science

June 1974

APPROVED:

Redacted for Privacy

Professor of Geophysics and Mathematics
in charge of major

Redacted for Privacy

Dean of School of Oceanography

Redacted for Privacy

Dean of Graduate School

Date thesis is presented April 24 1974

Typed by Susie Kozlik for Rex Wai-Yuen Tang

ACKNOWLEDGMENTS

I wish to thank my major professor Dr. Gunnar Bodvarsson for his guidance during my studies and his assistance and direction in preparation of this thesis.

I wish to thank Dr. Richard Couch, Mr. Bill McFarlane and Mr. Robert Whitsett for their help in this project. As members of the telluric field team Mr. McFarlane and Mr. Whitsett provided considerable assistance in explaining the records and calibrations.

Other members of the Geophysics Group who provided technical assistance are Mr. Michael Gemperle, Mr. John Bowers and Mr. Mike Cranford.

But most of all I wish to thank my father and mother for their encouragement and understanding.

This work was partially supported by:

Boeing Company

Weyerhauser Company

Pacific Power and Light Company

Department of Geology and Mineral Industries - State of Oregon, and the National Science Foundation.

TABLE OF CONTENTS

LIST OF FIGURES

LIST OF TABLES

GEOTHERMAL EXPLORATION BY TELLURIC CURRENTS IN THE KLAMATH FALLS AREA, OREGON

INTRODUCTION

The world's consumption of energy has about doubled every ten years during the past century. Due to the limited resources of fossil fuels, it will be difficult to maintain this rate of growth in the future without the development of new energy sources. Since many new methods of energy generation are still in the experimental stage, it is vital that interim resources within the realm of today's technologies be developed and exploitated. One such source is geothermal energy.

The use of geothermal energy offers many advantages. It is cheap and reliable. It has minimum environmental impact. Geothermal power plants can easily be incorporated into present electrical systems and are well within the capabilities of modern technologies. The main disadvantage of geothermal power generation is that the plants must be located near to the thermal resources since it is uneconomical to transport geothermal fluids over long distances.

Presently geothermal energy is being harnessed in many parts of the world. So far, most successful geothermal projects have been developed in industrial areas. However, since cheap, reliable local sources of energy are required for the developing economies, geothermal exploration is under way in many less developed countries. Possible uses of geothermal energy with particular reference to the

developing countries are discussed by Bodvarsson (1961, 1971). A summary of the status of world wide geothermal development has been given by Koenig (1973).

Characteristics of Geothermal Areas

The characteristics of individual geothermal areas are determined by the local heat sources and subsurface temperature distributions. The temperature field is controlled by rock conductivities, convective flows of fluids and by mass transfer by magma.

The world wide average specific heat flow is about 1.5 $\mu cal/cm^2$ sec (Lee and Uyeda, 1965). Since the conductivity of most rocks lie between 4 and 6 $\mu cal/cm\ sec\ ^oC$, the associated average temperature gradient is about $0.025\ ^oC/m$. In many regions of the United States, there exist areas of abnormally high conductive heat gradients (Sass et al., 1971).

In hydrothermal convective systems, heat is transferred by circulating ground water rather than by conduction. Convection takes place due to the expansion of the liquid at higher temperatures. The abnormally high temperatures at relatively shallow depths due to convective flows are reflected by a high surface temperature gradient which may exceed $1\ ^oC/m$. The gradient decreases rapidly with increasing depth. The temperature may at depths ranging from a few

hundred to more than a thousand meters attain a constant value which is referred to as the base temperature of the system (Bodvarsson, 1969).

Hydrothermal systems may be divided into two types, hot water systems and vapour dominated systems. Hot water systems are characterized by a water phase under pressure. Steam may be present in shallow low pressure zones but water is the medium by which heat is being carried from deep sources up to surface formations. The principal characteristics of hot water systems have been described by White et al. (1971) and may be summarized as follows:

1. Hot water springs are common.
2. Springs that are highest in temperature are also highest in gas and mineral concentrations.
3. A base temperature characterizes deeper parts of most hot water systems. This may approach 300 ^{o}C for water with low salinity and 400 ^{o}C for brines.

A minority of geothermal systems are of the vapor dominated type which produce dry or super-heated steam with no water phase. It has been hypothesized by White et al. (1971) that the vapor dominated type is formed by a low fluid recharge into a region of high heat supply. When the heat supply of a system is sufficient to boil off more than is replaced by the recharge, a vapor dominated system can be

formed. Geothermal fields at The Geysers and at Larderello are of this type. They are characterized by the following:

1. Fumeroles, mud volcanoes and acid leached areas are common.
2. Surface discharge of heat by steam is not significant since the ascending steam usually condenses before reaching the ground surface.
3. Reservoir temperature at a few hundred meters depth usually lie near 240°C.
4. Pressures in vapor dominated systems are 30 to 40 kg/cm^2.
5. During long term exploitation, the enthalpy of the steam produced increases since more saline water is being vaporized.

The vapor dominated systems are the most economical systems for commercial exploitation. Unfortunately, this type of system appears to be rare. High temperature hot water systems are also economically attractive although some additional problems including scaling and the disposal of hot water effluents are encountered.

United States Geothermal Resources

The western parts of the United States, including Hawaii, contain some of the world's greatest geothermal resources. Thermal areas are found in the states of Arizona, California, Idaho, Navada,

New Mexico, Oregon and Utah. In terms of known conventional methods of power generation, estimates of the geothermal potential of these areas vary from 400 to 4000 Mw-centuries (White, 1973). Rex and Howell (1973) claim that if newer techniques such as fracturing, deep drilling and heat exchange systems can be developed, recoverable energy reserves would amount to 4×10^6 Mw-centuries. This would be enough to meet the present United States electrical power needs for about 10^3 years.

The development of geothermal power generation in the United States has proceeded very rapidly during the past few years. Since the first turbine of 12.5 Mw was installed at The Geysers, California, in 1960, generating capacity there has grown to 400 Mw in 1974. This is now the largest geothermal power installation of its kind in the world. It is hoped that by 1980, the generating capacity will be enlarged to 1200 Mw. The direct use of geothermal heat for space heating has been applied most effectively in the city of Klamath Falls, Oregon, where some 500 buildings are heated by about 350 hot water or steam wells. Other areas in which geothermal development is being considered include Jemez Mountains, New Mexico and Imperial Valley, California.

ELECTRICAL METHODS IN THE EXPLORATION FOR GEOTHERMAL RESOURCES

The selection of geophysical methods for the exploration for geothermal resources depends on the many characteristics of the geothermal area. An optimum combination of geological, geophysical, hydrological and geochemical methods must be worked out. Needless to say, no one exploration technique is adequate for all stations (Combs and Muffler, 1973).

The objective of the direct geophysical methods is to delineate the thermal structure of the area under investigation. Based on extensive experience with electrical methods, it has been recognized that the resistivity of hot rock is considerably lower than that of the surrounding colder rock (Bodvarsson, 1950). For example, in New Zealand, hot areas have resistivities of less than 10 ohm-meters while the surrounding colder rock has resistivities of 100 ohm-meters or more (Banwell and McDonald 1965).

The resistivity of most types of rocks depend on the resistivity and amount of interstitial waters. The water is normally an electrolytic solution of various salts such as sodium chloride, calcium chloride, calcium bicarbonate and potassium chloride. The resistivity of these solutions decreases with an increasing concentration and also with increasing temperature. Moore (1966) found that water with a given salinity at 200^{o}C is five times more conductive than at 30^{o}C.

Thermal waters associated with geothermal areas usually contain relatively large concentrations of solutes. High temperature hot water systems may therefore be associated with a resistivity anomaly contrast involving factors of the order of ten. Conversely it may be expected that vapor dominated systems have higher resistivity than the surrounding rocks due to the reduced moisture content (Banwell, 1973).

The resistivities of solid rock at high temperatures are usually in the range of 100 to 5000 ohm-meters. At the melting point, the formation of an electrolytic melt causes the restivities to drop to a few ohm-meters. The presence of magma chambers at depths can therefore be detected with the help of electrical exploration methods.

The two principal types of electrical exploration methods are (1) the D . C. resistivity method and (2) the magneto-telluric method. There are a number of variants of each method. Some aspects of these two types of field methods will be discussed in the following with the emphasis on their application to geothermal exploration.

DIRECT CURRENT RESISTIVITY METHODS

Earth resistivities have been measured by many techniques. Most of the common methods apply a conductive coupling with the ground. Of all the electrical methods, the direct current method is conceptually the simplest. Essentially the field equipment consists of two parts, (1) the current circuit and (2) a device for measuring the electrical field strength.

An electric potential field is established when an electrical current is conducted into the ground by electrodes. This field is distorted by subsurface resistivity inhomogenieties. The objective of the exploration is to search for such anomalies in the electric field. Better known D. C. resistivity methods include the Wenner, the Schlumberger and the dipole methods.

In the Wenner configuration shown in Figure 1a, the electrodes are spaced equidistantly along a line. Measurements of the current and potential difference are made as the configuration is expanded symmetrically about a fixed center point. Deeper strata have an increasing effect on the potentials as the current electrode spacing grows larger. A description of the Wenner method has been given by Grant and West (1965).

Similarly, four collinear electrodes are also used in the Schlumberger configuration. The outer two electrodes are the current

sources and the inner two are the potential electrodes. The potential electrodes are located symmetrically about the center of the array and have a separation small compared with the total array length. The average voltage gradient is then the ratio between the measured voltage difference and the potential electrode separation. The separation of the current electrodes is gradually increased while the potential electrodes remain fixed. A sketch of a Schlumberger configuration is shown in Figure 1b.

Long lengths of heavy cable carrying currents at high voltages are a major safety problem in the case of long Wenner and Schlumberger configurations. Also great difficulties are encountered in laying out such cables. The long cables are avoided with the dipole-dipole technique shown in Figure 1c. Characteristics of this configuration is the large separation between the current electrode pair and the potential electrode pair. The four electrodes do not necessarily lie on the same line. Usually two orientations are used: (1) the polar configuration in which the dipoles are aligned and (2) the equatorial configuration in which the axis of the two dipoles are parallel but perpendicular to the base line. In both cases sounding is carried out by moving the potential dipole pair. The polar dipole configuration is shown in Figure 1c.

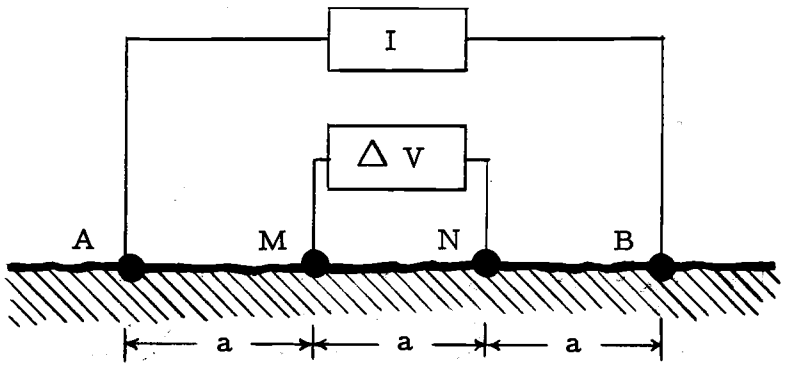

1a. Wenner configuration

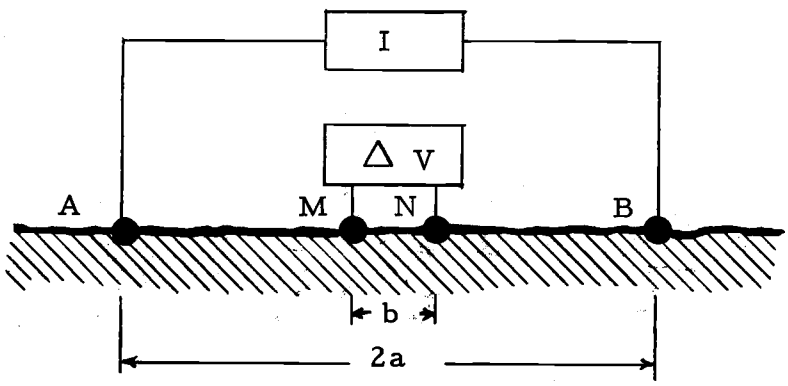

1b. Schlumberger configuration

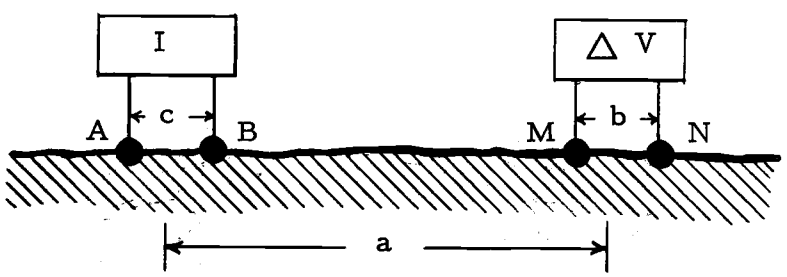

1c. Polar Dipole configuration

Figure 1. Direct current resistivity methods. A and B are the current electrodes, M and N are the potential electrodes and a is the characteristic spacing.

Direct Current Methods Over a Homogeneous Half Space

The simplest approach to the theory of the direct current techniques is obtained by considering the case of a homogeneous and isotropic half space. The theory of the electromagnetic fields is based on Maxwell's equations in the long wave approximation.

$$\nabla \times \bar{E} = \partial_t \bar{B} \tag{1}$$

$$\nabla \times \bar{H} = \bar{J} \tag{2}$$

$$\nabla \cdot \bar{B} = O \tag{3}$$

$$\bar{B} = \mu_o \bar{H} \tag{4}$$

$$\bar{E} = \rho \bar{J} \tag{5}$$

where $\bar{J}$ is the current density, $\bar{E}$ is the electric field, $\bar{H}$ is the magnetic intensity, $\bar{B}$ is the magnetic field, ρ is the resistivity of the media and μ_o is the magnetic permeability. Since we are considering the stationary case, equation (1) reduces to

$$\nabla \times \bar{E} = O \tag{6}$$

and hence E may be assumed to be the gradient of a scalar potential V:

$$\bar{E} = -\nabla V \tag{7}$$

Using Ohm's law (5) we obtain:

$$\bar{J} = -(1/\rho) \nabla V \tag{8}$$

The conservation of electrical charge gives:

$$\nabla \cdot \bar{J} = S \tag{9}$$

where S represents the current source strength per unit volume. Substituting equation (8) into (9) gives

$$-\nabla \cdot ((1/\rho)\,\nabla V) = S \tag{10}$$

Let the field point be P. In the case of a concentrated source of strength I at a point Q and assuming constant resistivity, we obtain:

$$-\nabla^2 V = \rho I \delta(P-Q) \tag{11}$$

where δ (P-Q) is the delta function centered at Q.

The solution of (11) is:

$$V(P) = \frac{I\rho}{4\pi r_{PQ}} \tag{12}$$

where r_{PQ} is the distance between P and Q.

The electric field E is given by:

$$\bar{E} = -\nabla V = \rho\, I\, r_{\bar{P}Q}/4\pi r_{PQ}^3 \tag{13}$$

For a current source on the surface of a homogeneous isotropic half space, the potential function V is:

$$V(P) = \frac{I\,\rho}{2\pi r_{PQ}}\,,\quad \bar{J}\,(P) = \frac{I\, r_{\bar{P}Q}}{2\pi r_{PQ}^3} \tag{15}$$

Since (10) is linear, the potential at an observation point M due to n concentrated surface sources, each with strength I_i is:

$$V(M) = \frac{\rho}{2\pi} \sum_{i=1}^{n} \frac{I_i}{r_{MQ_i}} \tag{16}$$

The Wenner, Schlumberger and dipole configurations all have 4 terminals. We assume that A and B are the current electrodes, while M and N are the potential electrodes.

The potential at a surface point M due to the current electrodes A and B is:

$$V(M) = \frac{I\rho}{2\pi}\left[\frac{1}{r_{AM}} - \frac{1}{r_{BM}}\right] \tag{17}$$

Similarly, the potential at a surface point N is:

$$V(N) = \frac{I\rho}{2\pi}\left[\frac{1}{r_{AN}} - \frac{1}{r_{BN}}\right] \tag{18}$$

Hence, the voltage difference measured between M and N is:

$$V(M) - V(N) = \Delta V = \frac{I\rho}{2\pi}\left[\frac{1}{r_{AM}} - \frac{1}{r_{BM}} - \frac{1}{r_{AN}} + \frac{1}{r_{BN}}\right] \tag{19}$$

For the Wenner configuration, the voltage difference is:

$$\Delta V = \frac{I\rho}{2\pi}\left[\frac{1}{a} - \frac{1}{2a} - \frac{1}{2a} + \frac{1}{a}\right] = \frac{I\rho}{2\pi a} \tag{20}$$

For the Schlumberger configuration, the voltage difference is:

$$\Delta V = \frac{I\rho}{2\pi}\left[\frac{1}{a-b/2} - \frac{1}{a+b/2} - \frac{1}{a+b/2} + \frac{1}{a-b/2}\right]$$

$$= I\rho\ \left(\pi(a^2/b - b/4)\right)^{-1} \tag{21}$$

Similarly, the voltage difference for the polar dipole configuration is:

$$\Delta V = \frac{I\rho}{2\pi}\left[\frac{1}{a+c/2-b/2} - \frac{1}{a-c/2-b/2} - \frac{1}{a+c/2+b/2} + \frac{1}{a-c/2+b/2}\right]$$

$$= I\rho\ \left[\pi(a^3/b^2 - b)\right]^{-1} \tag{22}$$

where b is the separation between M and N and c is the separation between A and B. In the above equation it is assumed that b=c.

Apparent Resistivity

Based on equations (20), (21), and (22), in the proceeding section, the mutual resistance measured for the four types of configurations can be expressed:

$$\rho = K \Delta V/I \tag{23}$$

where K is a geometric constant characteristic of the configurations used.

In most situations the conditions of isotropy and homogeniety are rarely fulfilled. Resistivities usually vary with depth and in lateral directions. Under such homogeneous conditions, equation (23) above defines an average or apparent resistivity of the half space. The averaging is over a volume that depends on the electrode spacing. At larger spacings, deeper resistivities will have an increasing effect on the apparent resistivity values.

Apparent Resistivity for the Two Layer Case

A full treatment of the derivation of the potential function for the two layer case is given by Grant and West (1965), Van Nostrand and Cook (1966) and Keller and Frischknecht (1966). Two methods can be used to derive the potential functions,(1) the Hankel transform method, and (2) the theory of images.

Using the Hankel transform method, the potential on the ground at a surface point M is:

$$V(M) = \frac{I\rho}{2\pi}\left(\frac{G(AM, k)}{AM} - \frac{G(BM, k)}{BM}\right) \tag{24}$$

where G(r, k) is an inverse Hankel transform:

$$G(r, k) = 1 + 2kr\int_0^\infty (e^{2\lambda h} - k)^{-1} J_0(\lambda r)\, d\lambda \tag{25}$$

where h is the first layer thickness, r is the radius and k is the reflection coefficient:

$$k = \frac{\rho_2 - \rho_1}{\rho_2 + \rho_1} \tag{26}$$

where ρ_1 and ρ_2 are resistivities of the first layer and the second layer respectively.

The apparent resistivity with the Wenner configuration is then:

$$\rho_a = 2\pi\, a\, \Delta V/I = \rho_1\,(2G(a, k) - G(2a, k)) \tag{27}$$

As an illustration of a special case we show in Figure 2 the computed apparent resistivity curves for the above four types of configurations for a two layer earth with a reflection coefficient k = -0.8.

To resolve the second layer resistivity in the two layer case, the electrode spacing must be large enough so that the initial curvature of the apparent resistivity can be derived with sufficient accuracy. In the cases illustrated in Figure 2, the curvature for the various configurations can be distinguished with some certainty only when $\rho_a/\rho_1 \leq 0.7$. Hence the Wenner and Schlumberger configurations

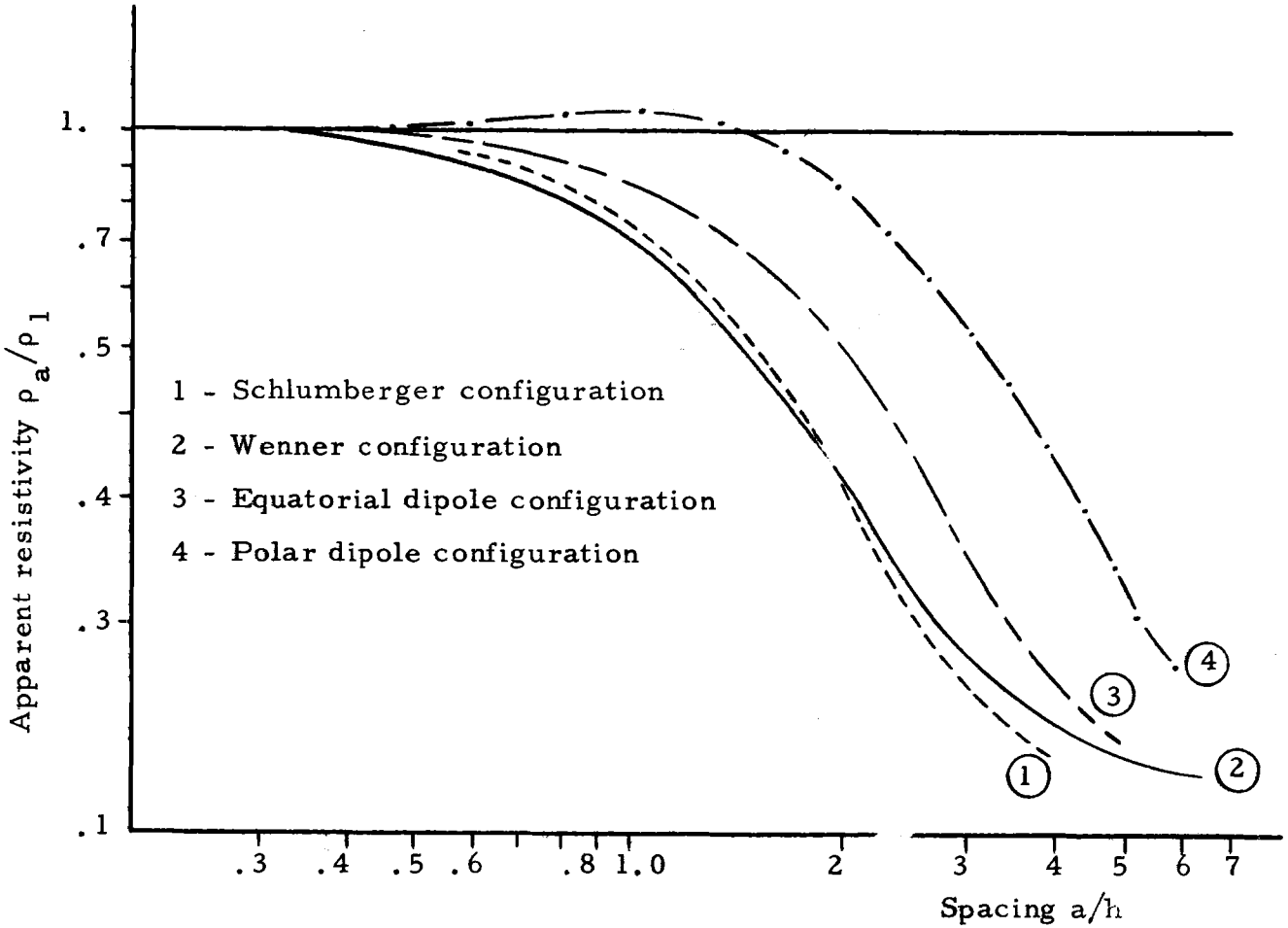

Figure 2. Apparent resistivity curves over a two-layer earth with k=-0.8.

must then have a minimum spacing approximately equal to the first layer thickness and the polar dipole configuration must have a dipole spacing equal to at least three times the first layer thickness.

Parabolic Resistivity Distribution

Bodvarsson (1950) has investigated the case of a parabolic resistivity distribution in a half space:

$$\rho(z) = A\, z^{-n} \tag{28}$$

where A is a constant, z is the depth and n is an integer. By solving Laplace's equation for this case, Bodvarsson found that the potential at a distance r_{PQ} from a concentrated surface current source of strength I at a point Q is

$$V(P) = AI\,(2\pi\, r_{PQ}^{n+1})^{-1} \tag{29}$$

In the case of a Wenner configuration the measured potential difference between the potential electrodes is then:

$$\Delta V = V(M) - V(N) = \frac{AI}{2\pi}\left[1/a^{n+1} - 1/(2a)^{n+1} - 1/(2a)^{n+1} + 1/a^{n+1}\right]$$

$$= \frac{AI}{\pi a^{n+1}}\left[1 - 1/2^{n+1}\right] = \frac{I\rho(a)}{2\pi a}\left[2 - 1/2^{n}\right] \tag{30}$$

Hence, the apparent resistivity at a spacing a is directly proportional to the actual resistivity at the depth a:

$$\rho_a = \rho(a)\left[2 - (1/2^n)\right] \tag{31}$$

For the Schlumberger configuration the potential difference between potential electrodes with a spacing b is:

$$\Delta V = \frac{AI}{2\pi}\left[\frac{1}{(a-b/2)^{n+1}} - \frac{1}{(a+b/2)^{n+1}} - \frac{1}{(a+b/2)^{n+1}} + \frac{1}{(a-b/2)^{n+1}}\right] \quad (32)$$

In the special case b = 0. 2a, the above equation becomes:

$$\Delta V = \frac{AI}{\pi a^{n+1}}\left(\frac{20^{n+1}}{99^{n+1}}\right) \quad (33)$$

and the apparent resistivity for this configuration is:

$$\rho_a = \pi(a^2/b - b/4)\,\Delta V/I$$

$$= \frac{A}{a^n}\left(\frac{20}{99}\right)^n = \rho(a)\left(\frac{20}{99}\right)^n \quad (34)$$

Compared with the Wenner configuration it is seen that the initial curvature of this sounding curve is smaller.

For the polar dipole configuration the voltage measured between the potential electrodes is:

$$\Delta V = \frac{AI}{2\pi}\left[\frac{1}{(a+c/2-b/2)^{n+1}} - \frac{1}{(a-c/2-b/2)^{n+1}}\right.$$

$$\left. - \frac{1}{(a+b/2+c/2)^{n+1}} + \frac{1}{(a-c/2+b/2)^{n+1}}\right]$$

where c is the current electrode separation. For the case where b=c=0. 1a, the above equation can be simplified to the form:

$$\Delta V = -\frac{AI}{2\pi a^{n+1}}\left[\frac{110^{n+1} + 90^{n+1}}{99^{n+1}} - 2\right] \quad (35)$$

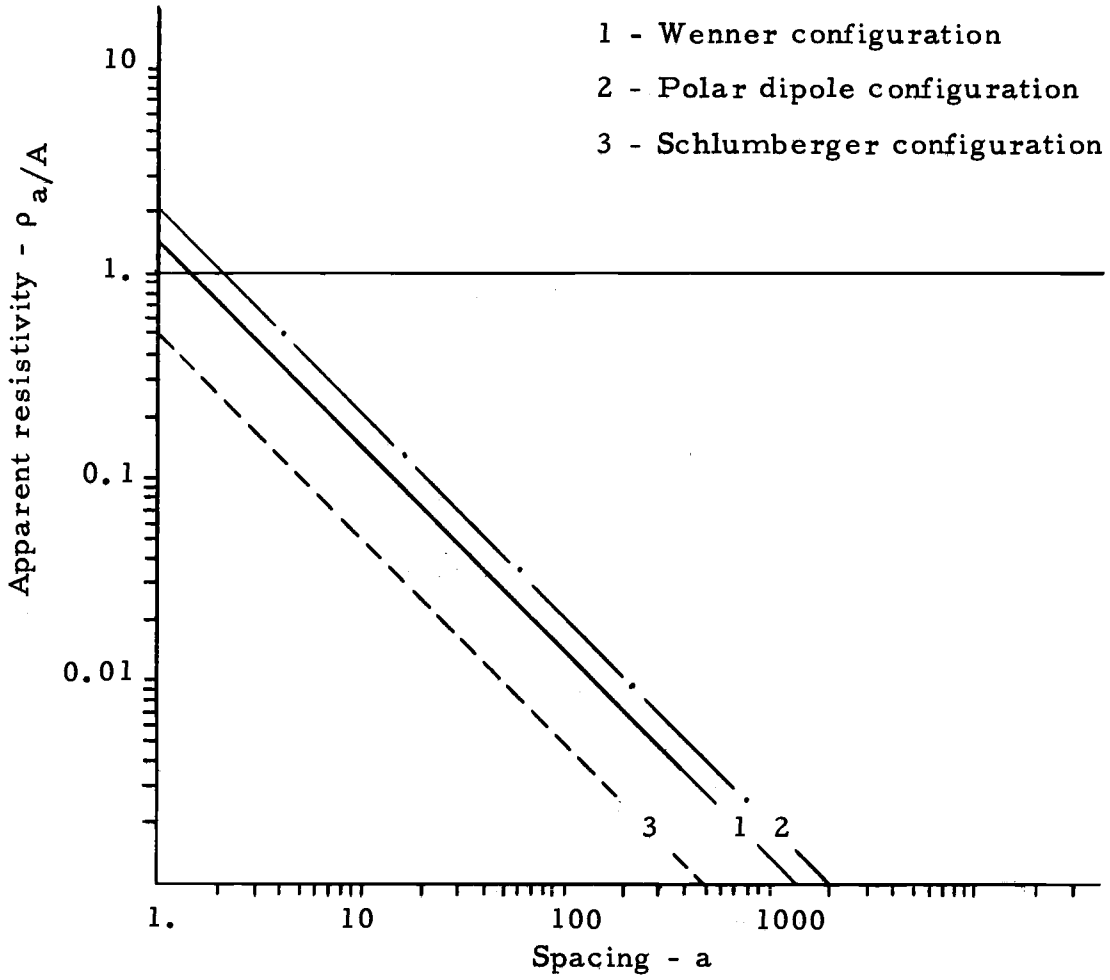

Figure 3. Apparent resistivity curves for direct current configurations over a semi-infinite half space with a parabolic resistivity distribution $\rho = A/z$.

and the apparent resistivity is:

$$\rho_a = \rho(a)\left[50\frac{110^{n+1} + 90^{n+1}}{99^{n+1}} - 100\right] \qquad (36)$$

For a parabolic resistivity distribution, the apparent resistivity curves all have the same form as the actual resistivity-depth curve and differ only by a multiplicative constant. For the Wenner configuration, this constant is nearly 2 for large n values while for other configurations, the constant varies considerably. In Figure 3 the apparent resistivity curves for the different configurations are shown for a parabolic resistivity distribution with an exponent n = 1.

Noise Limitations

In investigating the performance of the various electrode configurations at noisy field conditions, we will concentrate on the influence of the ambient telluric noise field with periods greater than one second. In the western coastal regions of the United States, noise levels at periods up to 100 seconds vary from 0.1 to 10 millivolts per kilometer. In southern Oregon, telluric amplitudes measured on the present project have under most conditions a range of 0.1 to 1.0 millivolts per kilometer. This is equal to 10^{-7} to 10^{-6} volts per meter.

For a spacing of Ca between the potential electrodes, where C is a constant and a is the characteristic spacing of the configuration,

the amplitude of the noise field would be in the range of 10^{-7}Ca to 10^{-6}Ca volts. Assuming an acceptable signal / noise ratio of 10, the minimum acceptable voltage between the potential electrodes for a noise level of 1 millivolt per kilometer must therefore be:

$$\Delta V = 10^{-5}\text{Ca volts} \tag{37}$$

For a low noise level of 0.1 millivolts per kilometer, the signal must have a minimum amplitude of:

$$\Delta V = 10^{-6}\text{Ca volts} \tag{38}$$

By applying equations (37) and (38) and the apparent resistivity equations derived for the various electrode configurations, we can now derive a relationship between the spacing and the minimum required current.

Based on equations (20), (21) and (22), and assuming a homogeneous and isotropic half space, the following relations hold for the Wenner configuration:

$$a = \frac{I\rho}{2\pi\Delta V} \tag{39}$$

for the Schlumberger configuration:

$$a = \frac{I\rho}{2\pi\Delta V}\left(C^{-1} - C/4\right)^{-1} \tag{40}$$

and the polar dipole configuration:

$$a = \frac{I\rho}{\pi\Delta V}\left(C^{-2} - C\right)^{-1} \tag{41}$$

where a is the characteristic spacing and Ca is the distance between the potential electrodes. Since the average noise voltage between the potential electrodes is proportional to the spacing a, we find that for a given signal / noise ratio and noise level there is for each direct current configuration a minimum applicable value of $I\rho$. Substituting (37) and (38) into equations (39), (40) and (41), we obtain:

$$(I\rho)_{min} = K_c a^2 \qquad (42)$$

where I is the source current, ρ is the resistivity and K_c is a constant depending upon the electrode configuration and the signal / noise ratio.

Assuming that for the Schlumberger configuration b = 0.2a and for the dipole configuration b = c = 0.1a, a noise level of 0.1 and 1.0 mv/km and a signal / noise ratio of 10, the minimum $I\rho$ values are shown in Figure 4. Having obtained a minimum value of $I\rho$, we can for each given a and ρ derive a minimum current I to be applied in order to exceed the assumed voltage signal / noise ratio.

There are, on the other hand, practical limitations to the current which can be applied to the ground. This depends on the surface resistivity and the size and number of the electrodes applied. The limitations on the current from above and on the signal / noise ratio from below have the effect that there is a definite limitation to the maximum characteristic spacing at which measurements with a desired precision can be carried out. A few relevant results will be given below.

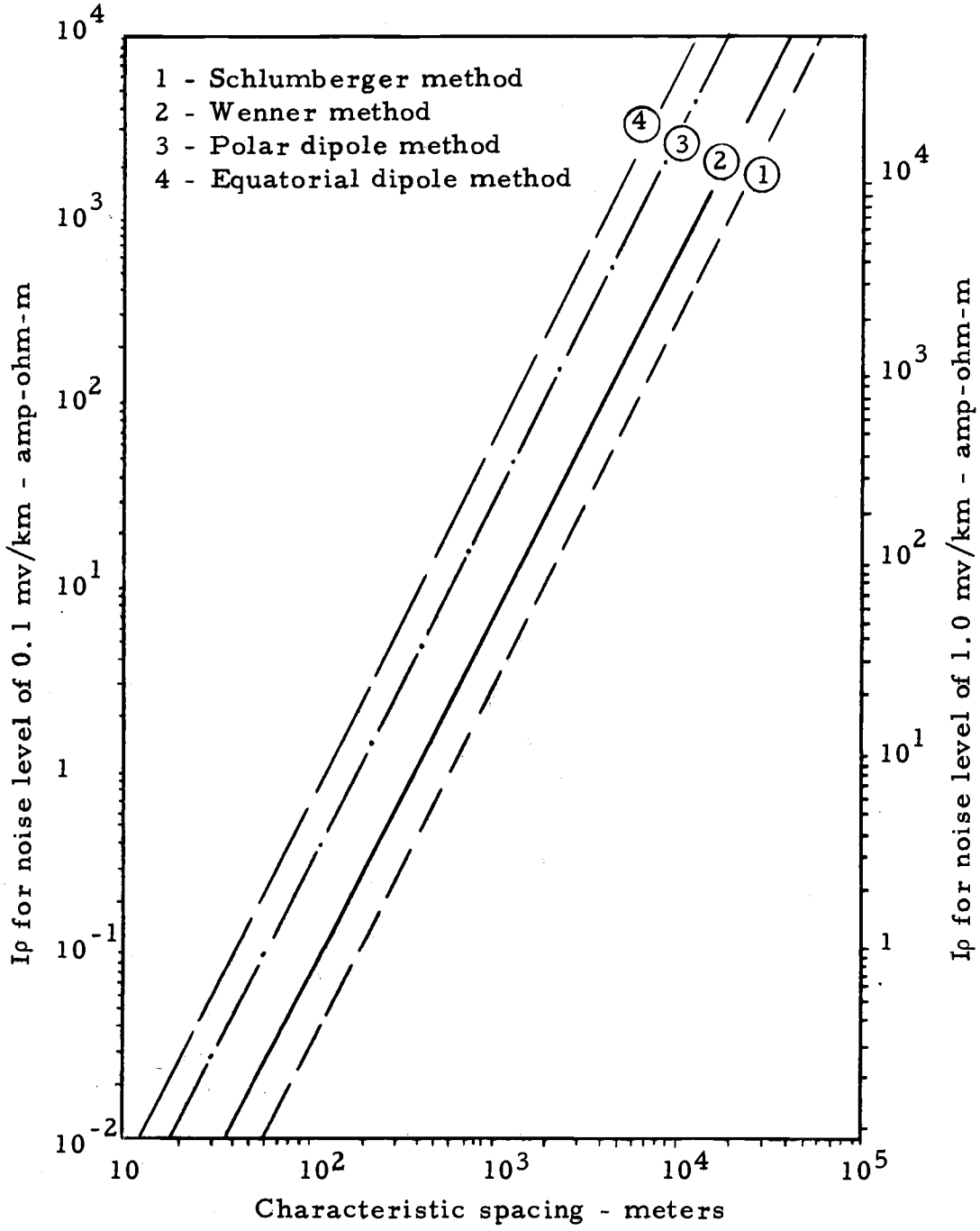

Figure 4. Minimum Iρ values for the direct current resistivity methods at a given signal/noise ratio and noise level.

To obtain an estimate of the currents which can be applied to the ground, we will consider the case of a cylindrical current electrode inserted into the ground. The contact resistance is (Sunde, 1949):

$$R_c = (\rho / 2\pi L)[\mathrm{Log}(4L/d) - 1] \qquad (43)$$

where L is the length of the electrode, d is the diameter and ρ is the resistivity of the ground around the electrode. Since the resistivity of surface sand and soil often amounts to several thousand ohm-meters, we will assume a minimum of 1000 ohm-m. The total contact resistance of two current electrodes of L = 1 m and d = 0.025 m would then be about 1000 ohms. If the maximum applied voltage is 500 volts, the resulting maximum current will be 0.5 amps. Using this value of the current and the data given in Figure 4, we can now derive a maximum characteristic spacing for a given half- space resistivity, electrode configuration and noise level. The results for the signal / noise ratio and the two noise levels assumed above are shown in Table 1 and 2 below.

Table 1. Relationship between maximum applicable characteristic spacing and resistivity for a source current of 0.5 amp, a signal / noise ratio of 10 and a noise level of 0.1 mv/km.

Subsurface resistivity	Wenner spacing	Schlumberger	Polar dipole spacing	Equatorial dipole spacing
1 ohm-m	300 m	400 m	140 m	100 m
10	1000	1400	450	250
100	3000	4000	1500	1000
1000	10000	14000	4500	2500

Table 2. Relationship between maximum applicable characteristic spacing and resistivity for a source current of 0.5 amp, a signal / noise ratio of 10 and a noise level of 1.0 mv/km.

Subsurface resistivity	Wenner spacing	Schlumberger spacing	Polar dipole spacing	Equatorial dipole spacing
1 ohm-m	95 m	125 m	45 m	32 m
10	320	450	140	80
100	950	1250	470	320
1000	3200	4500	1400	800

For the Schlumberger, Wenner and equatorial dipole configurations the maximum depth at which a second layer resistivity of a two layer case may be estimated is approximately equal to the characteristic spacing. For the polar dipole configuration, the depth of resolution is less than a third of the characteristic spacing.

The values in the above tables indicate quite strongly the limitations on the application of the ordinary D.C. resistivity methods to low resistivity areas such as geothermal areas where resistivities of the order of 1 to 25 ohm-meters may be involved. The exploration depth is severely limited.

The above consideration has been limited to interference by telluric current noise. Other noise sources, such as geological noise, that is, small and medium scale surface resistivity inhomogenieties are equally important. Data on geologic noise conditions are not available, but this factor can be treated along somewhat

similar lines as above. Geologic noise contributes a further limitation on the exploration depth which can be attained by the conventional D. C. resistivity methods.

THE MAGNETO-TELLURIC METHOD

The magneto-telluric method utilizes the geomagnetic micropulsation field as a source. The most prominant activity occurs in the 20 to 40 second period band which is referred to as the $P_{c,3}$ activity. The $P_{c,3}$ oscillations exhibit large variations in amplitude with latitude and a characteristic diurnal pattern. Despite this, individual events and packets of micropulsation activity may occur at almost exactly the same time over the world. A thorough review of magnetic micropulsations has been given by Jacobs(1971).

The first paper dealing with the magneto-telluric method appeared in 1950 and was authored by Tikhonov (1950). He realized that geomagnetic pulsations and telluric currents, observed at the surface of the earth, must be related. Using the low frequency pulsations, Tikhonov used the telluric-magnetic impedance ratio to derive the resistivities and thicknesses of crustal and upper mantle layers at Tuscon, Arizona, and Zui, USSR. Subsequent to this, Cagniard (1953) published a paper on the theory and technique of magneto-telluric prospecting which has been extensively referenced since. In this paper, Cagniard makes the assumption that the geomagnetic micropulsations are plane waves interacting with a layered semi-infinite space. He derived the relationship between E_x, the electrical field component, and H_y, the orthogonal magnetic field component observed at the surface of the half space and computed a set of master curves

for two and three layer cases with various parameters. By comparing experimental apparent resistivity curves with these master curves, quantitative results on the resistivities at various depths can be obtained.

The method has been extensively developed since and applied to the geophysical exploration of many areas. For a discription of the theory, papers by Berdichevsky and Brunelli (1959), Wait (1961) Price (1962) and Chetaev (1960) are useful. A good summary of the magneto-telluric method may also be found in Keller and Frischknecht (1966). Examples on the application of this method in geophysical exploration and case histories may be found in the papers by Vozoff et al. (1966, 1968, 1972).

Theory

The theory of the magneto-telluric method can be outlined as follows. The amplitude of the geomagnetic micropulsations source field is assumed to be homogeneous, horizontal and unidirectional. This assumption has been challenged previously (Price, 1962) but it has been established that this holds true under most conditions (Vozoff and Ellis, 1966). The incident field is partially reflected and partially absorbed by the earth which is assumed to be a layered semi-infinite half space.

On the basis of Maxwell's equations (1) to (5), we can derive the relationship between the magnetic field $\overline{B}$ and the electric field $\overline{E}$ in the half space. We place our (x, y) plane in the surface of the solid with the z axis downward, assume that the fields are proportional to $e^{-i\omega t}$ and that:

$$\overline{B} = (O,\ B_y(z),\ O) \tag{44}$$

$$\overline{E} = (E_x(z),\ O,\ O) \tag{45}$$

equation (2) gives:

$$E_x = -(\rho/\mu_o)\frac{dB_y}{dz} \tag{46}$$

and from equation (1) we obtain:

$$\frac{dE_x}{dz} = -i\omega B_y \tag{47}$$

Differentiating this equation with respect to z and substituting from equation (46) results in:

$$\frac{d^2E_x}{dz^2} - s^2E_x = 0 \tag{48}$$

where $s = (i\omega\mu/\rho)^{1/2}$. The real part of s is the reciprocal of the skin depth d which is defined as the depth at which the field amplitude has decreased to e^{-1} of the surface value. The skin depth for various frequencies and resistivities is given in Figure 5.

The orthogonal electrical and magnetic field components E_x and B_y in a homogeneous conductor can be written as:

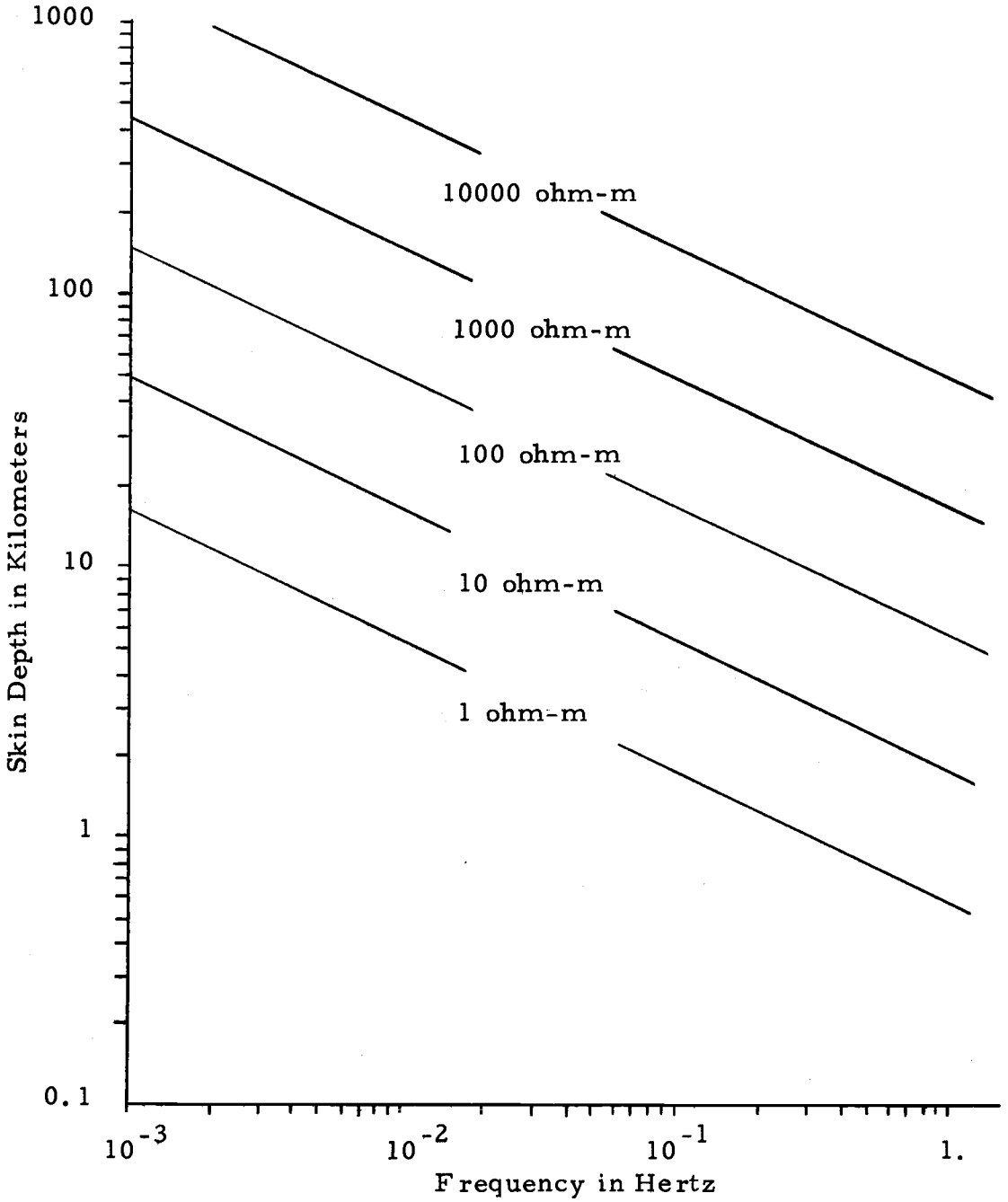

Figure 5. Skin depth $d=(2\rho/\mu_o\omega)^{1/2}$ for different resistivities and frequencies.

$$B_y = B_{oy} e^{-i\omega t} e^{sz} \tag{49}$$

$$E_x = E_{ox} e^{-i\omega t} e^{sz} \tag{50}$$

$$E_{ox} = \left(\frac{i\omega\rho}{\mu_o}\right)^{1/2} B_{oy} \tag{51}$$

where the first subscript indicates the field values at the surface of the earth. Using (5) we can see that the resistivity of the conductor is given by:

$$\rho = \frac{i\mu_o}{\omega}\left(\frac{|E_{ox}|}{|B_{oy}|}\right)^2 \tag{52}$$

In terms of real field amplitudes, where E is measured in millivolts per kilometer and B in gammas, the result reduces to

$$\rho = 0.2\, T\left(\mu_o \frac{|E_{ox}|}{|B_{oy}|}\right)^2 \Omega\text{-m} \tag{53}$$

where $\mu_o = 1$.

In the case of a uniform earth, the electric field amplitude leads the magnetic field amplitude by 45°. If the resistivity varies with depth, equation (52) defines an apparent resistivity ρ_a which is a function of the period. An apparent resistivity curve is obtained by plotting the ρ_a against the period. A theoretical apparent resistivity may be calculated exactly for any desired layering of the half-space. In the two layer case, the formula is (Berdichevsky and Brunelli, 1959):

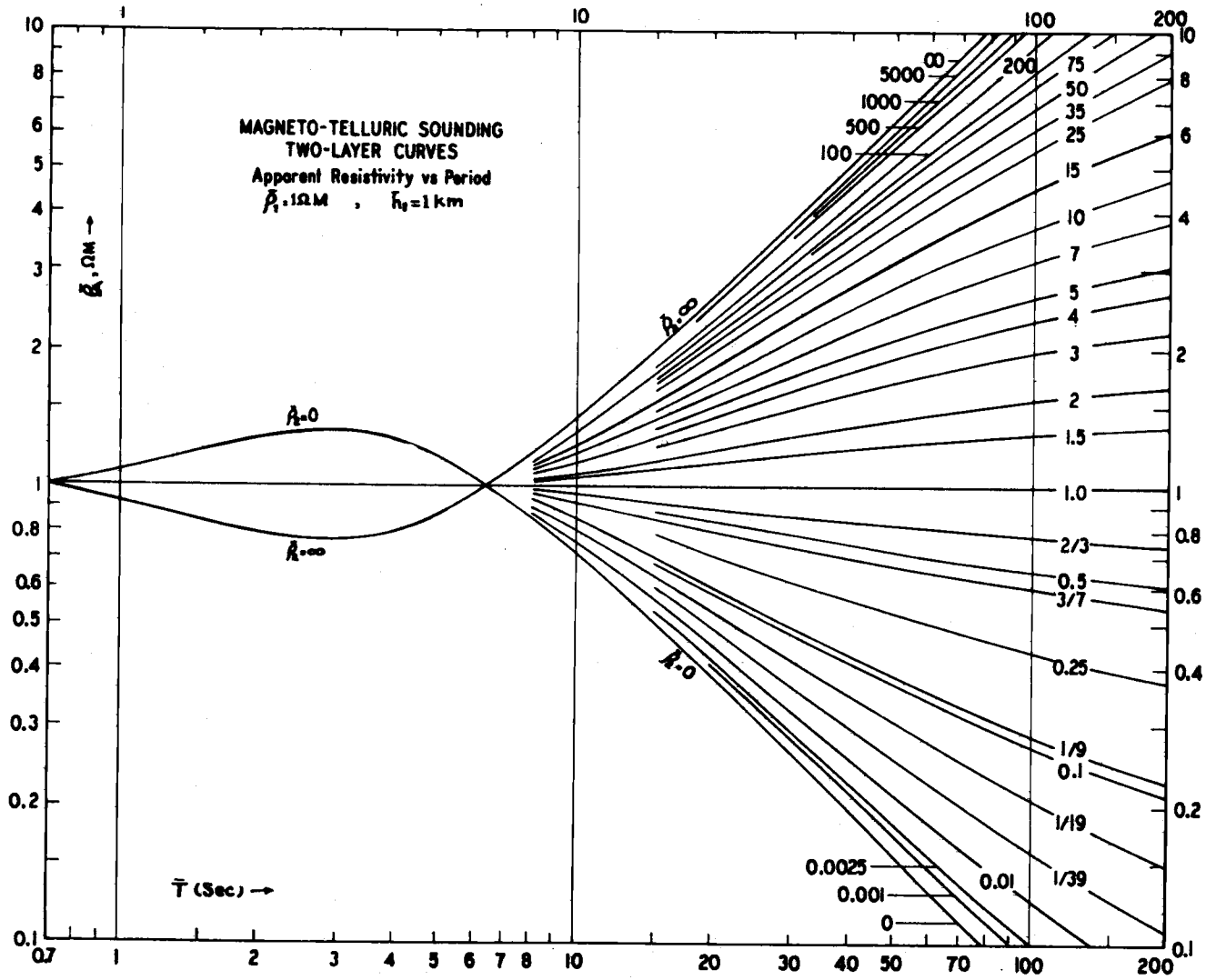

Figure 6. Magneto-telluric, two layer standard curves from Yungul (1961).

$$\frac{E_{ox}}{B_{oy}} = -\frac{i\omega}{\mu s_1} \coth \left[s_1 h_1 + \operatorname{arcoth} \left(\frac{\rho_2}{\rho_1}\right)^{1/2} \right] \qquad (54)$$

where the subscripts refer to the two individual layers. The theoretical resistivity curves for this case are shown in Figure 6. By comparing the experimental resistivity curves with the theoretical curves, the actual resistivities can be determined. This technique of interpretation is called the curve matching method.

Comparison of Magneto-Tellurics with Direct Current Methods

In comparing the magneto-telluric method with the direct current conduction method, the following should be emphasized:

1. The magnetic source field is generated by sheet-like electric currents in the ionsphere which are of great extent. The resulting magnetic field and the induced telluric currents are frequently uniform over a large area. All geometric effects due to electrode configurations are therefore avoided.
2. For relatively deep investigations, the magneto-telluric field equipment is considerably lighter than the D. C. conduction equipment and the total field effort in man-hours is smaller.

3. As a consequence of (1) and the low frequency involved, the depth of penetration is much greater than that of the conventional D.C. conduction method.

4. The greater depth penetration is of particular interest in the exploration of geothermal resources where D.C. conduction work is often very difficult because of the high conductivities which reduce measurable voltage signals. This problem has been discussed in Chapter 3 above. Moreover, magneto-telluric investigations are unaffected by surface layers of low conductivity which pose problems in D.C. conduction work because of high electrode contact resistance.

5. On the other hand, the magneto-telluric method has the disadvantage that the source field is variable with regard to amplitude, frequency and uniformity. The interpretation is often subject to considerable uncertainty and the resolution may be poor.

The $P_{c,3}$ micropulsation band appears especially suited for deep geoelectrical prospecting. There is sufficient signal energy available in this band. Since the telluric electric field is affected by resistivity inhomogenieties in the upper crust, the mapping of the telluric field strength therefore provides a convenient and effective regional reconnaissance method in the prospecting for geothermal

resources. This technique is particularly useful in the case of deep sources without surface display and it is applicable as a convenient and economical reconnaissance technique in any region of geothermal prospect.

OREGON STATE UNIVERSITY MAGNETO-TELLURIC FIELD PROGRAM

In 1971, the Geophysics Department at Oregon State University initiated a telluric current field program in a region along the Klamath Graben in southern Oregon. The telluric field data was obtained at each site by an array of three telluric field sensors to be described below. The three components of the magnetic field were recorded at a fixed base station in Corvallis 220 km from the center of the area under investigation. It is assumed that the magnetic pulsation field is sufficiently homogeneous over this distance so that the telluric field records can be processed on the basis of the Corvallis station data alone. The use of a fixed magnetic base station is of convenience since it saves considerable field effort.

Approximately 20 hours of data were collected before the program was discontinued due to the lack of funding. Figure 7 shows the project area and the sites at which telluric records were made. Sites were chosen on the basis of assessibility, minimum electrical noise interference and absence of interferring metallic structures such as water pipes. Of the original 17 sites, only 10 sites provided useful data due to recorder malfunction. For our purposes, the series of sites from Miess Lake in California to Swan Lake in the northeast are most important since these stations provide an apparent resistivity profile across the Klamath Graben.

In 1972, similar telluric studies, were made at various stations in Central and Eastern Oregon. The station locations are shown in Figure 8. The results from Central Oregon and from the stations near the town of Vale in Eastern Oregon are being included in this paper. The Vale region has apparently a history of some geothermal activity as evidenced by the wide spread hydrothermal mineralization.

Physiography and Location of Project Area

The physiography of the Klamath Falls area is complicated and not much is known about its geologic history. A useful description has been given by Peterson and McIntyre (1970) from which the following is derived.

The area is characterized by extensive extrusions of Pliocene basalt flows which are overlain by a complex suite of more recent rocks such as cinders, basalts and tuffs. Most of this area has been recently folded and faulted with a north-westerly strike. Due to the recent volcanic activity, the geology appears to be favorable for the presence of geothermal resources. The basalt flows at depth may contain fractures that provide conditions for hot water and steam reservoirs. The fault zones facilitate water recharge and the covering depositions may provide insulation to trap heat and steam. Many parts of the area have anomalously high heat flows and hot springs are found

in a number of locations. It appears likely that there are intrusive bodies at depth which form the sources of these thermal manifestations.

There are mainly two centers with an abnormally high geothermal gradient, that is, (1) the area around the city of Klamath Falls and (2) the South Klamath Hills area. In the city, 350 wells have been drilled for the heating of 500 houses, apartments, schools, businesses and the Oregon Technical Institute. Thermal water with a temperature greater than 150°F is recovered from an area not less than 10 square miles. In certain locations temperatures of 250°F are encountered at depths of 100 to 300 feet. A detailed account of geothermal activity has been given by Peterson and McIntyre (1970). There is therefore an evidence for geothermal potential in the project area that warrants further investigation.

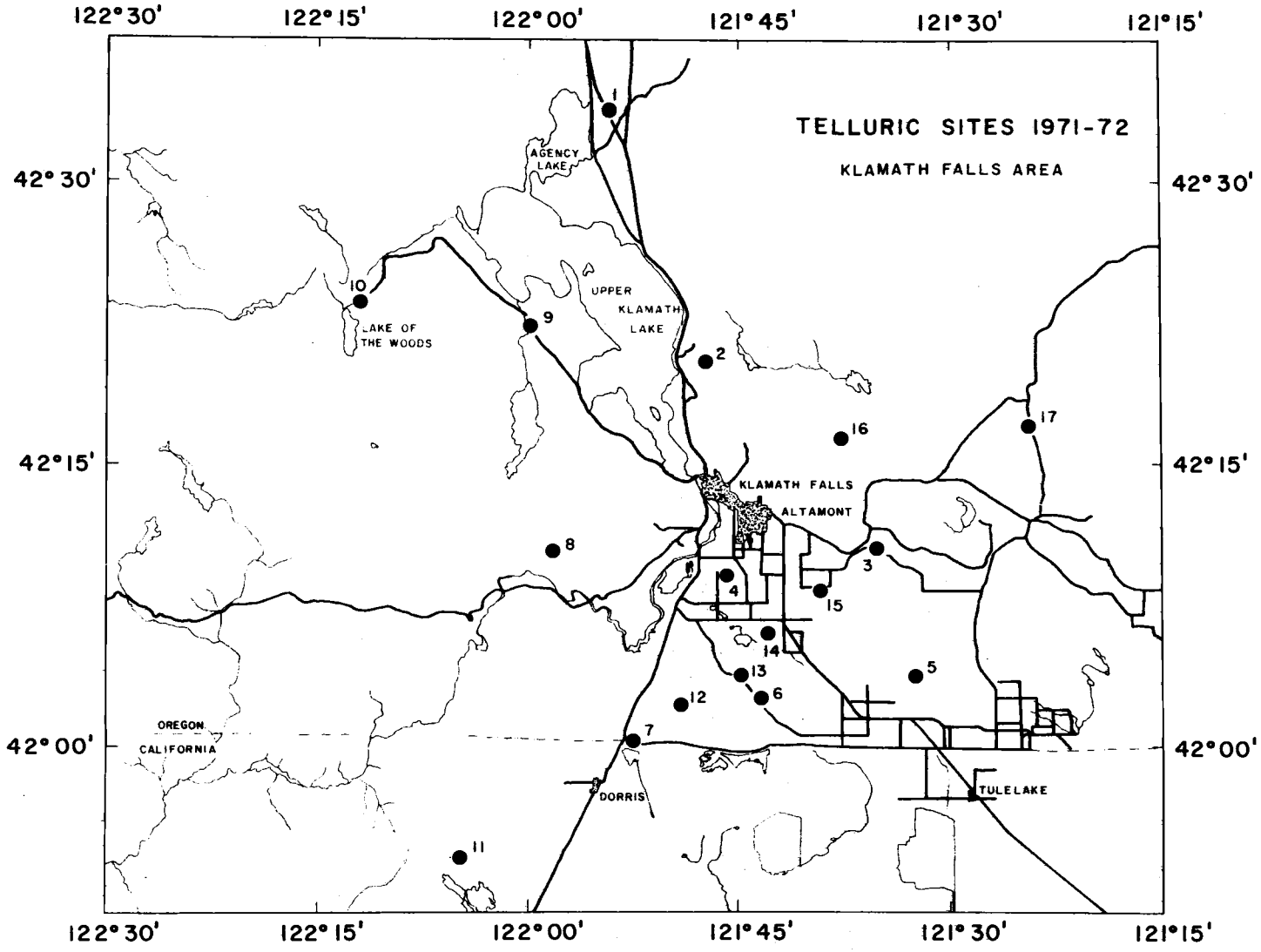

Figure 7. Telluric sites in Klamath Falls.

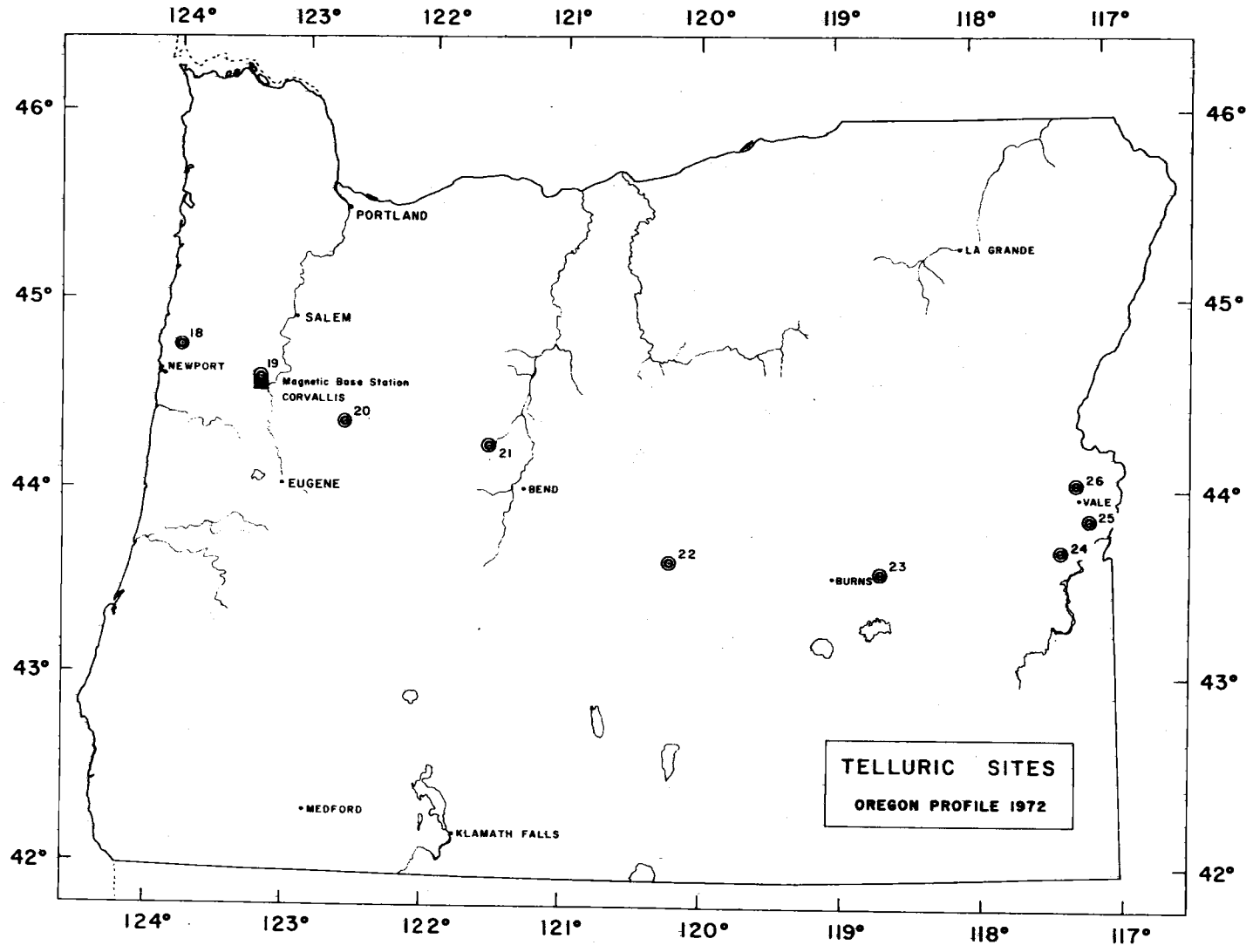

Figure 8. Telluric sites across Oregon.

INSTRUMENTATION

The magneto-telluric system used in the present study consists of two distinct parts, the telluric and the magnetic systems. The sensors for the magnetic base station located at Corvallis consist of three mutually orthogonal coils. The portable telluric field sensors are simple lead electrodes. The output signals from both systems are amplified and recorded on multitrack strip chart recorders.

Magnetic Sensors

The magnetic sensors consist of three multiturn mumetal cored induction coils each with 4.8×10^5 turns of wire. The B_x coil has a horizontal axis parallel to the local magnetic north-south direction. The B_y coil has its axis horizontal and parallel to the local magnetic east-west direction. The B_z coil has a vertical axis. The complete set of coils is placed in the open and connected to the amplifier-recorder system inside the World Wide Standardized Seismic Network Station vault at Corvallis, Oregon. Accurate timing was provided by the station crystal clock. A detailed description on the construction of the coils may be found in a paper by McNicol and Johnson (1964).

Telluric Sensors

The telluric sensors consist of three lead metal probes inserted into the ground at a spacing of about 300 meters. In the Klamath Falls area, E_x was placed approximately parallel to the local geological strike with a direction about 35^o west off the geographical north-south. At other field stations, E_x was approximately north-south. The other telluric axis, E_y, was always placed orthogonal to E_x. Each probe consists of a piece of metallic lead plate 5mm thick, 600mm wide and 1000mm long. These were rolled into a tube 200mm in diameter and buried in the ground. The electrode setup has the form of an 'L' with the length of the arms ranging from 200 meters to 500 meters depending upon the environment. The connecting wires to the amplifiers consist of insulated copper wire soldered to the probes. Such long cables inevitably pick up some small amount of 60 cycle hum, particularly near high voltage transmission lines. However, lower frequencies are unaffected due to the presence of a damping device on the strip chart recorders. With the 'L' spread, the corner electrode was used as the common ground for the two recording channels. The D.C. field is blocked out with a non-polar 20 μfarad capacitor. The outputs were amplified and recorded on four track strip chart recorders.

Signal Amplifiers

The signals from all five sensors (three magnetic and two telluric) are amplifed by Medistor type A60 voltmeters. A full description of the circuit and mode of operation of the Medistor amplifiers is given in the manufacturer's instruction manual (Model A-60, Microvoltmeter).

The frequency response of the amplifiers is given in Figure 9 for both the 'slow' and 'fast' position. Normally the 'slow' position was used. It can be seen that the response is flat within the range of interest which is 0.1 to 0.01 sec^{-1}.

Strip Chart Recorders

The amplified magnetic micropulsations were recorded on a two track Texas Instrument strip chart recorders. Each track had an approximate width of 100mm and the chart speed was fixed at 20mm/min. The pens were ink type and caused some maintenance problems. The response characteristics of the sensor-amplifier-recorder system is shown in Figure 10. It can be seen that there is a sharp decline in gain at frequencies less than 0.05 sec^{-1}. This is due to the induction pickup characteristics of the magnetic sensors. Following a maximum at 0.1 Hz the gain falls off due to the amplifier characteristics and losses in the core of the pickup coil.

Upon amplification the telluric fields were recorded on a four track Mechanics For Electronics (M. F. E.) strip chart recorder with a hot pen. Each track has an available width of 50 mm.. Chart speed was adjustable from 10mm/min to 1000mm/min but only 50mm/min was actually used. The differences between the magnetic and telluric data speeds caused some difficulties in the data analysis. The M. F. E. recorder is provided with amplification for each channel and 50 mv/mm was usually preferred. The gain of the telluric sensor, amplifier and recorder system is more linear than the magnetic system gain as can be seen in Figure 10. A full description of the M. F. E. strip chart recorder is given in the manufacturer's instruction manual (Model M24, Mechanics for Electronics, Wilmington, Mass. 1973).

The reliability of the equipment used in this project was not too good. Repairs were required for both the telluric and magnetic systems on separate occasions and calibrations had to be redone each time. Wherever possible the latest or final calibration was applied in the processing of the records.

Calibration

The calibration of the magnetic system was made by using an artificial oscillating magnetic field. This was generated by a Heath coil driven by the Fairchild oscillator at various frequencies. This

coil was set up at a distance of approximately 10 meters parallel to the sensor to be calibrated. The calibration was performed with various gain settings of the amplifiers and recording combination.

Previous calibration of the magnetic system was performed at the Boeing Company in Seattle by McNicol and Johnson (1964) by using a rotating permanent magnet with a varying rotational speed. The magnetic data aquisition system is shown in Figure 11 and the telluric data aquisition system is shown in Figure 12.

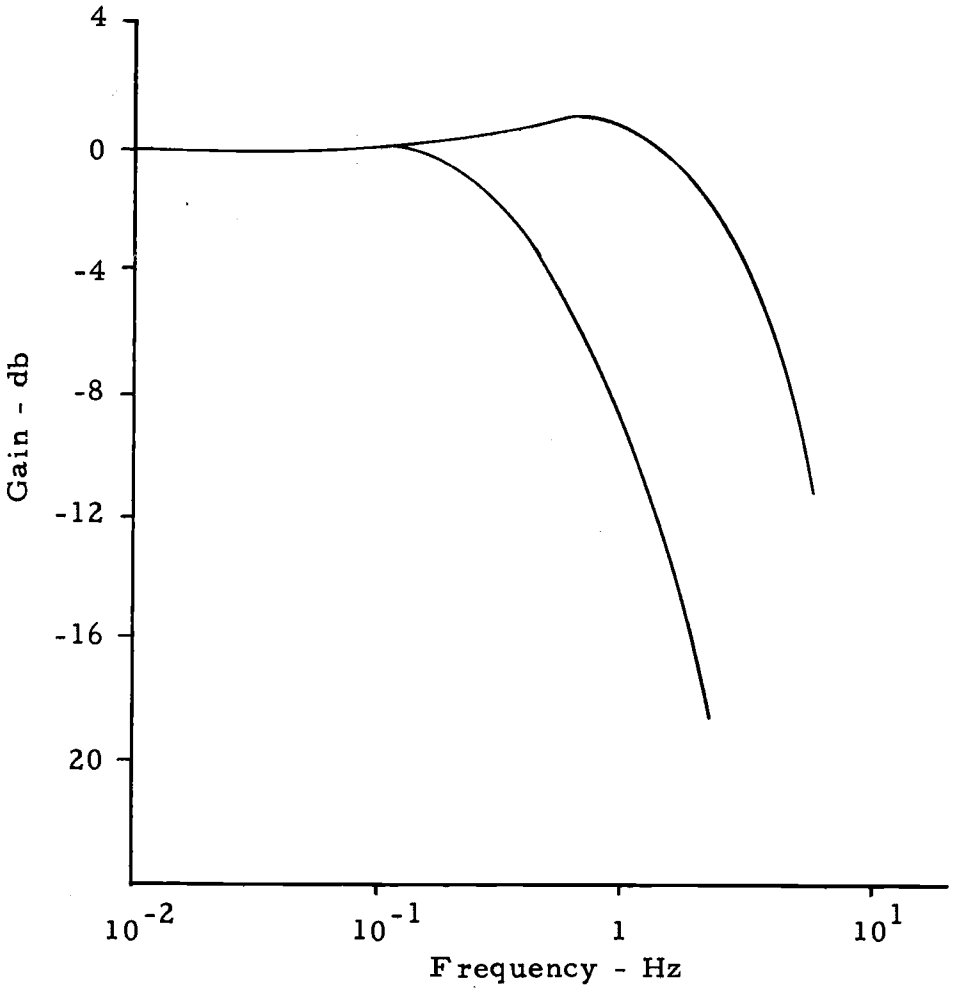

Figure 9. Gain of Medistor Amplifier.

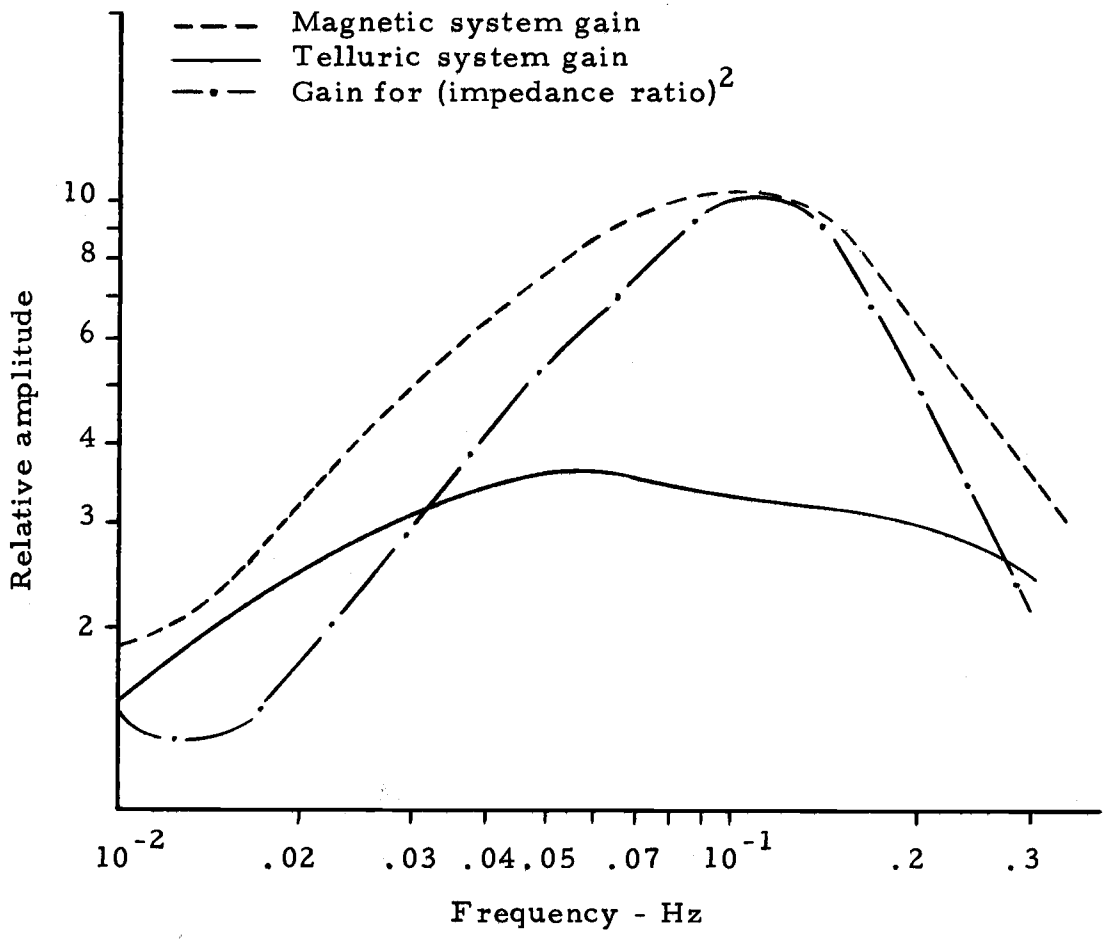

Figure 10. Example gain of sensor-amplifier-recorder systems.

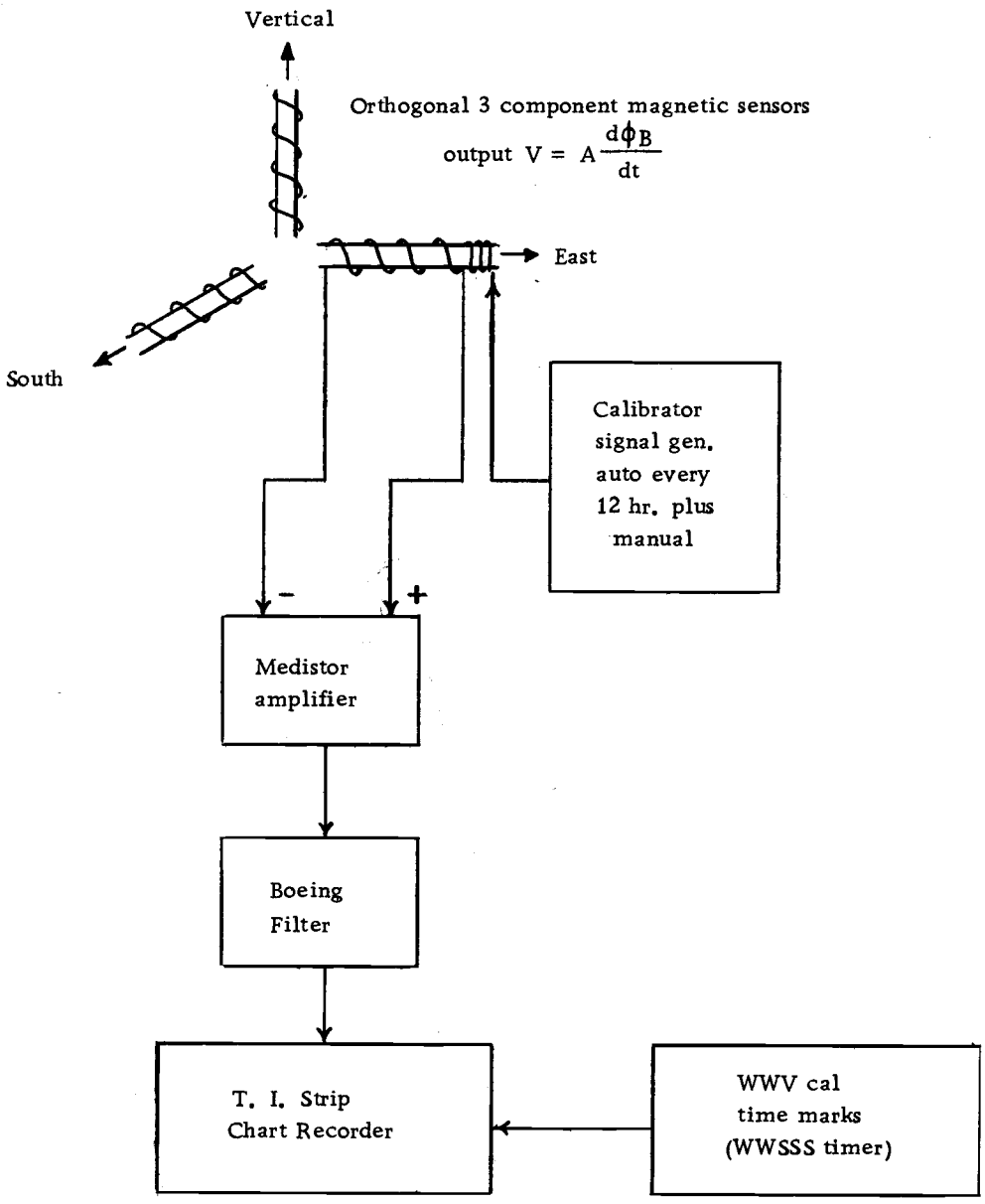

Output: Voltage versus time proportional to magnitude of micropulsations

Figure 11. Magnetic data aquisition system.

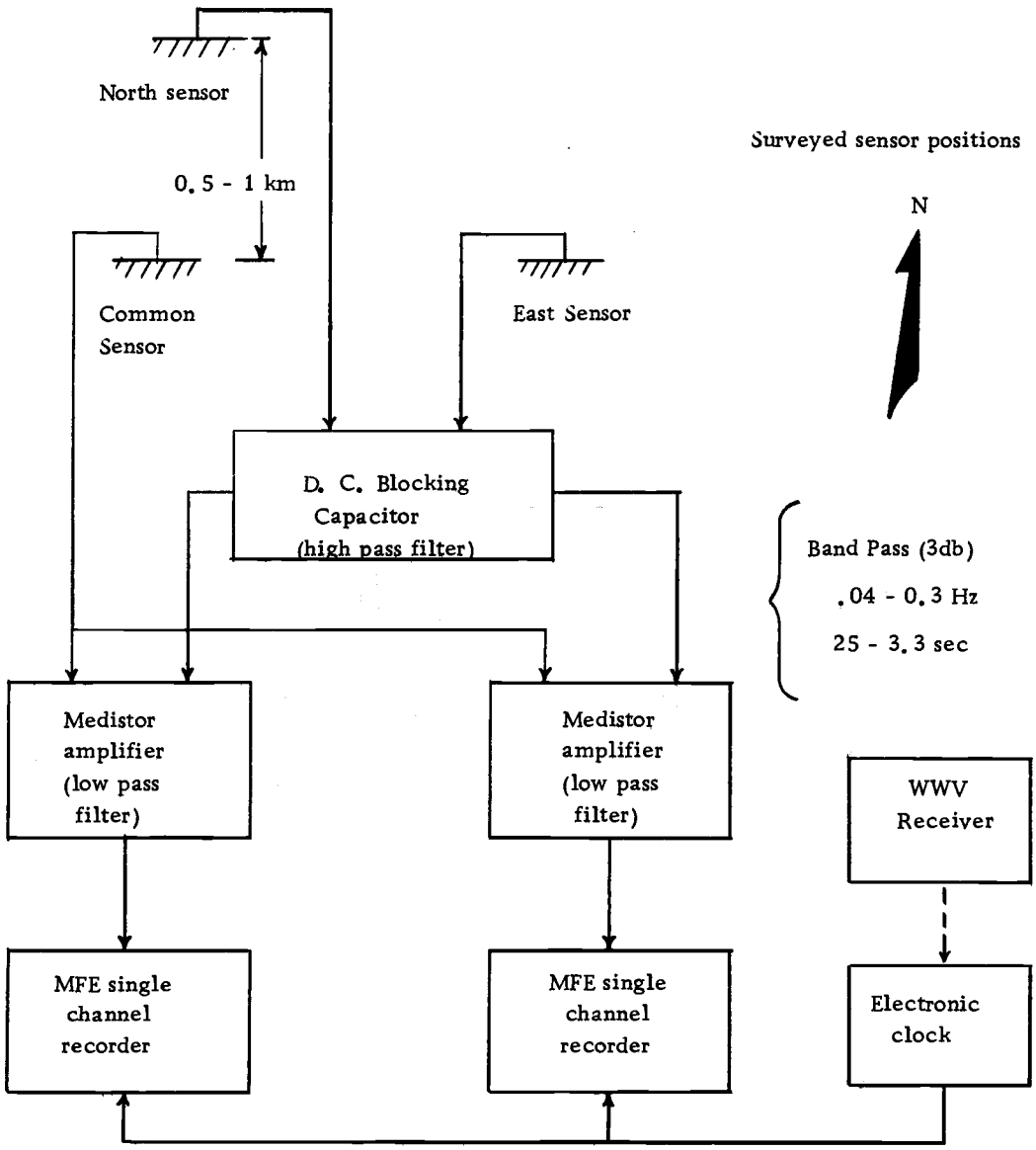

Output: Voltage versus time, each absolutely calibrated
usually expressed mv/km

Figure 12. Telluric data aquisition system.

MAGNETO-TELLURIC DATA PROCESSING

The data was analysed on the basis of two methods, spectral analysis and individual event analysis. Power spectral analysis involved hand digitization of all records. Fourier components, power spectra, and cross correlation functions were subsequently computed using the Oregon State University Control Data Corporation (CDC3300) digital computer on the basis of an *ARAND package of subroutines (Ballance, Baughman and Ochs, 1973). Because of the relatively low overall coherence between the magnetic and telluric field data, the power spectral analysis gave rather unsatisfactory results. It was therefore decided to rely primarily on individual event analysis in the deriving of apparent earth resistivities.

Spectral Analysis

Hand digitization had to be used because of the different recording speeds of the magnetic and telluric and strip chart recorders. The digitization was carried out in the Civil Engineering Department at Oregon State University. A coordinate digitizer used in cartography was used.

The interval chosen for digitization was either 2 seconds or 4 seconds depending on the amplitude of the recorded signal. The small interval was chosen with regard to the large variations in some of the

records. Since each station has 4 data records, two magnetic records B_x and B_y and the two field telluric records E_x and E_y, a data length of 1000 seconds would require the digitization of 2000 points. Considering that a record interval of 0.025 inches is equivalent to a digitization interval of 2 seconds a considerable effort is required.

The first step in the spectral analysis was to derive the Fourier coefficient of each set of magnetic and telluric records. The FOURTR subroutine of *ARAND was used. The Fourier expansion of the original data curve F(t) is given by the following equation:

$$F(t) = R_o + 2 \sum_n R_n \cos(\omega_n t + \phi_n) \qquad (55)$$

where ω_n is the angular frequency, t is time, ϕ_n are phase angles and R_n are Fourier coefficients. The coefficients were calculated with a frequency increment of 0.01 Hertz from zero to the maximum frequency depending upon the digitization interval.

The purpose of this work was to provide an initial investigation of the spectra and coherency between the magnetic and telluric field records. As an example, the Fourier components of the B_x and E_y magneto-telluric fields of station 13 (South Klamath Hills) are shown in Figure 13. The figure indicates a relatively good correlation between these two Fourier transform records. On both curves prominent peaks occur in the 0.01 to 0.05 frequency band of the $P_{c,3}$ activity.

The extremely large amplitudes at less than 0.01 Hertz is due to the gain curve which vanishes at zero frequency (Figure 10). Amplitudes fall off at higher frequencies which is characteristic of micropulsations noise. The magneto-telluric records B_x and E_y from site 13 (South Klamath Hills) are shown in Figure 14 and indeed the similarity is striking. Unfortunately, most stations did not exhibit such a high degree of magnetic-telluric correlation.

The magneto-telluric records for site 11 (Poe Valley) are shown in Figure 15. The Fourier coefficients for the B_x and E_y components obtained in the case of this station are shown in Figure 16. Though first impression indicates a fair correlation between peaks and troughs, the magnetic and telluric records exhibit rather poor coherency. Careful examination of the Fourier coefficients shows that the correlation in the important 0.03 to 0.05 Hz frequency band is poor. Due to low correlation at this station further analysis was impossible and apparent resistivity values were therefore not obtained.

The next step in the spectral analysis was to obtain the power spectral density curves for the two pairs of magneto-telluric variations for each station. The SPECTIC subroutine of *ARAND was used. In Figure 17 the spectrum for the magnetic field components E_x and B_y are shown in the case of station 13 (South Klamath Hills). The curve is relatively smooth and its amplitude is inversely proportional to the frequency. Peaks exist in the $P_{c,3}$ activity frequency band. Power

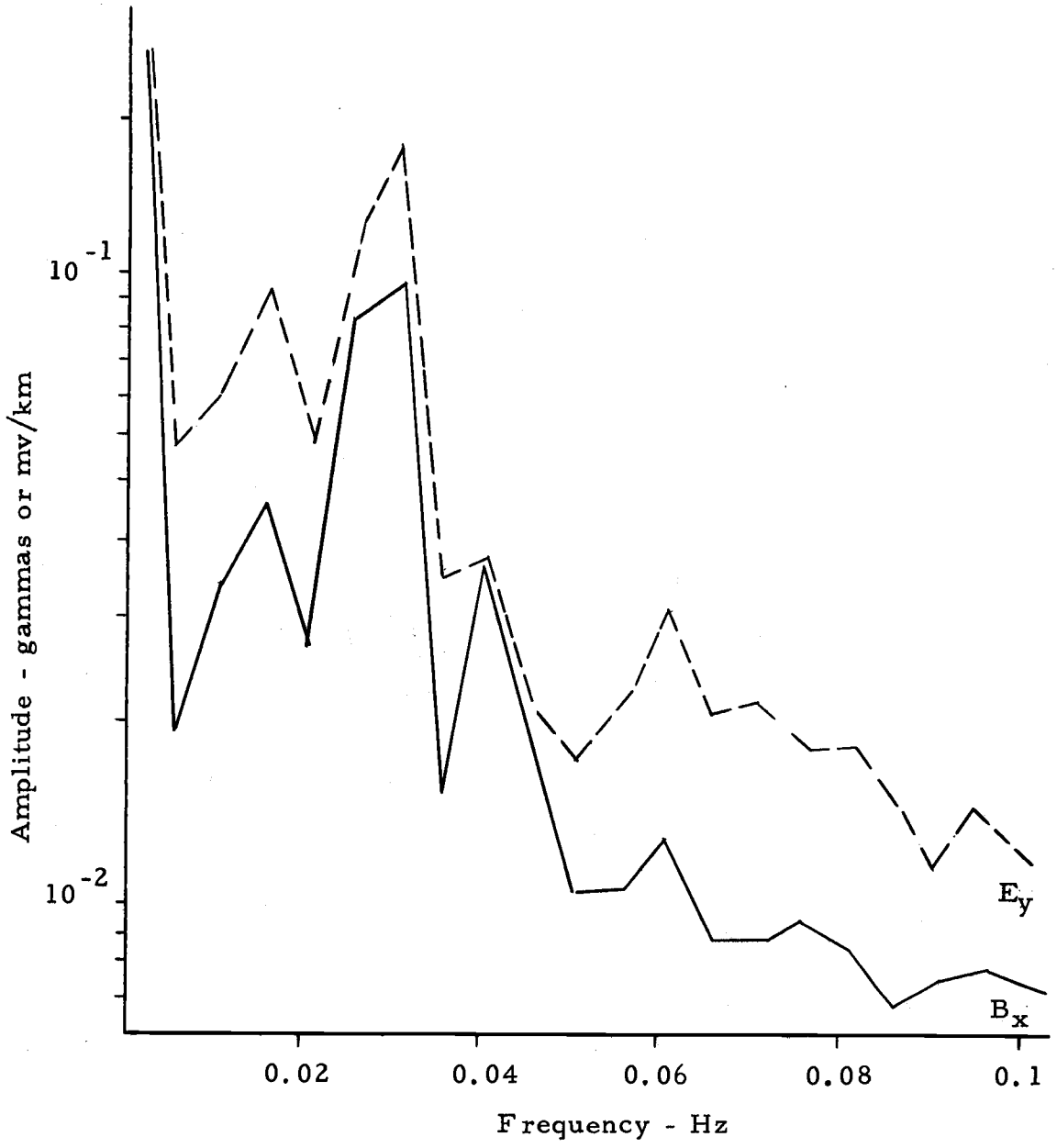

Figure 13. Fourier coefficients for station 13 (South Klamath Hills).

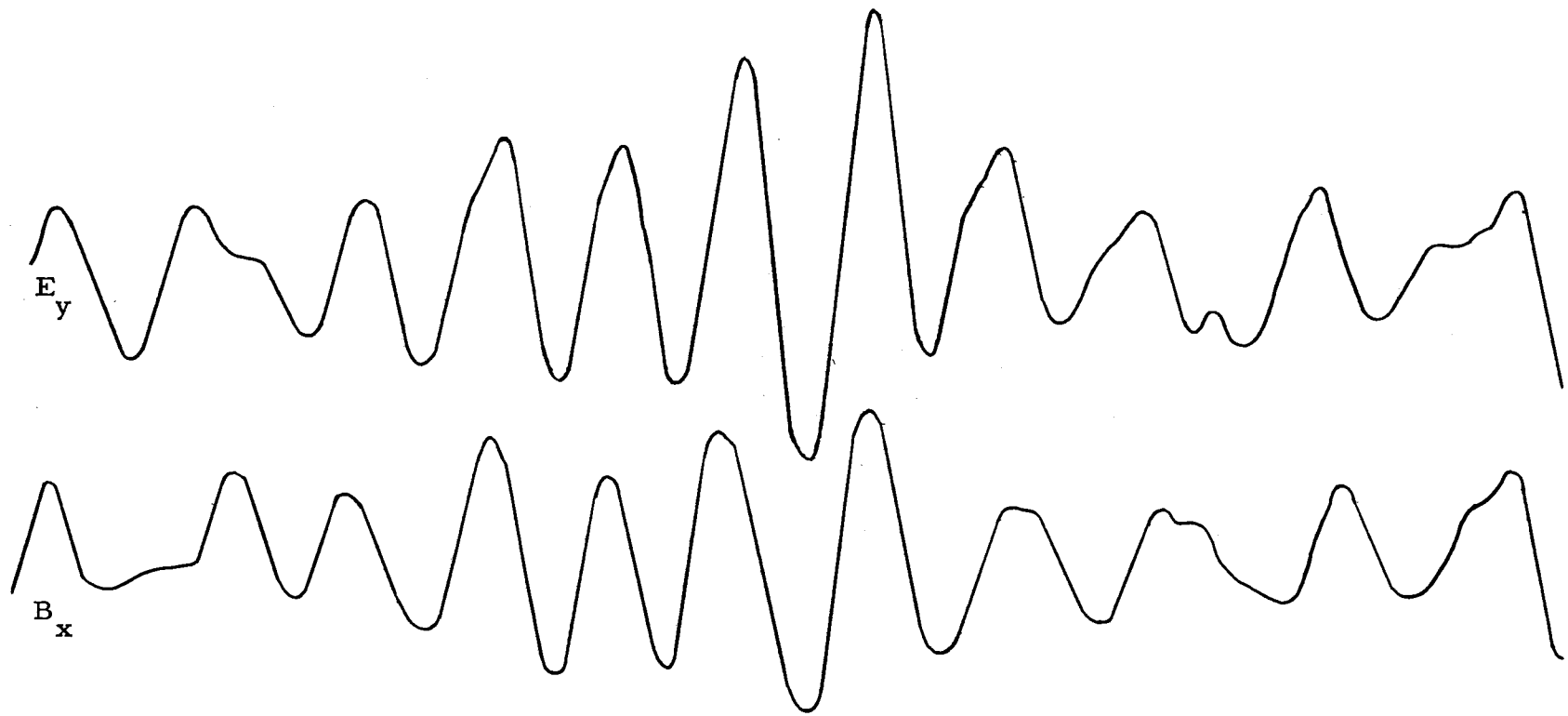

Figure 14. Magnetic-telluric records for station 13 (South Klamath Hills).

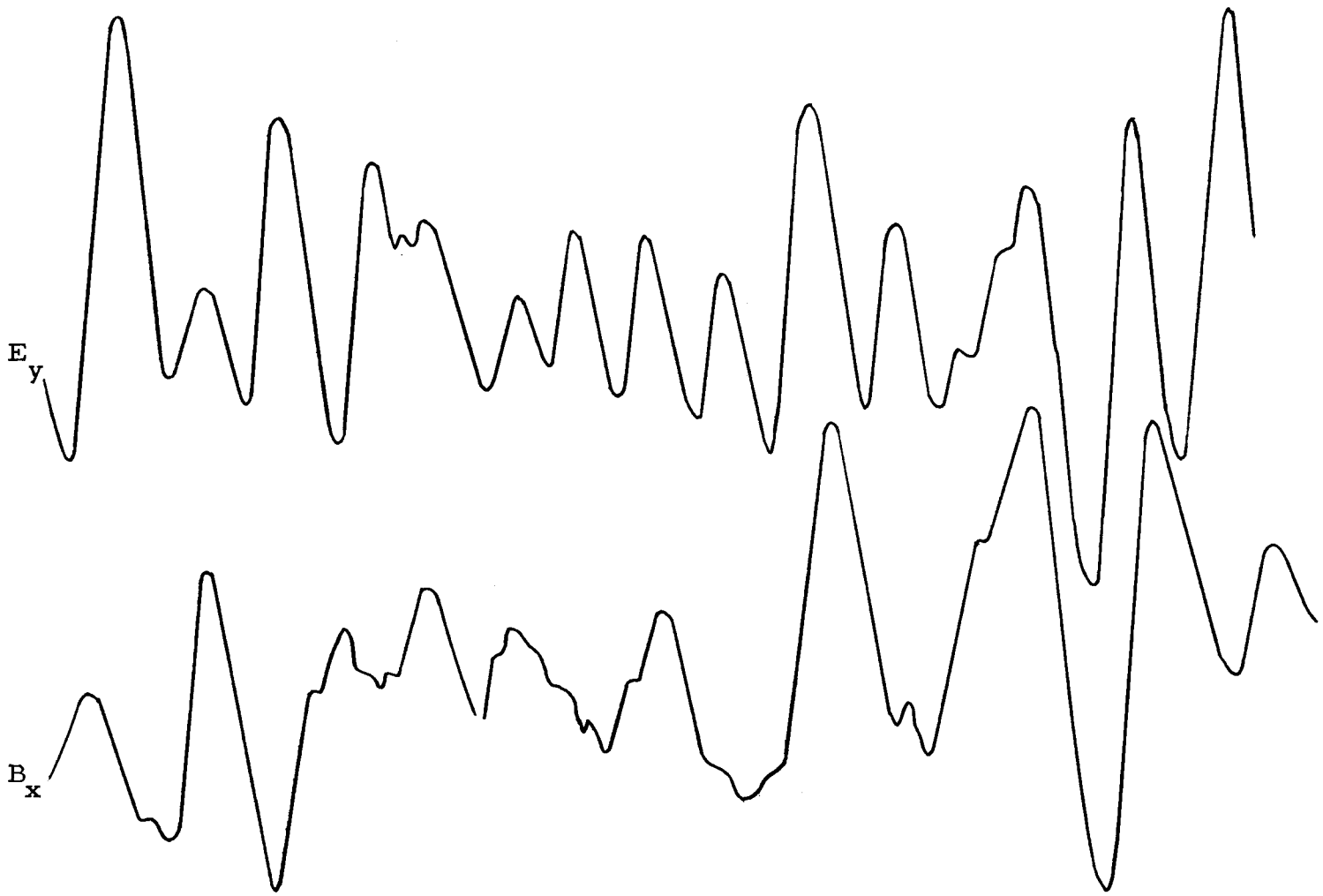

Figure 15. Magnetic-telluric records for station 11 (Poe Valley).

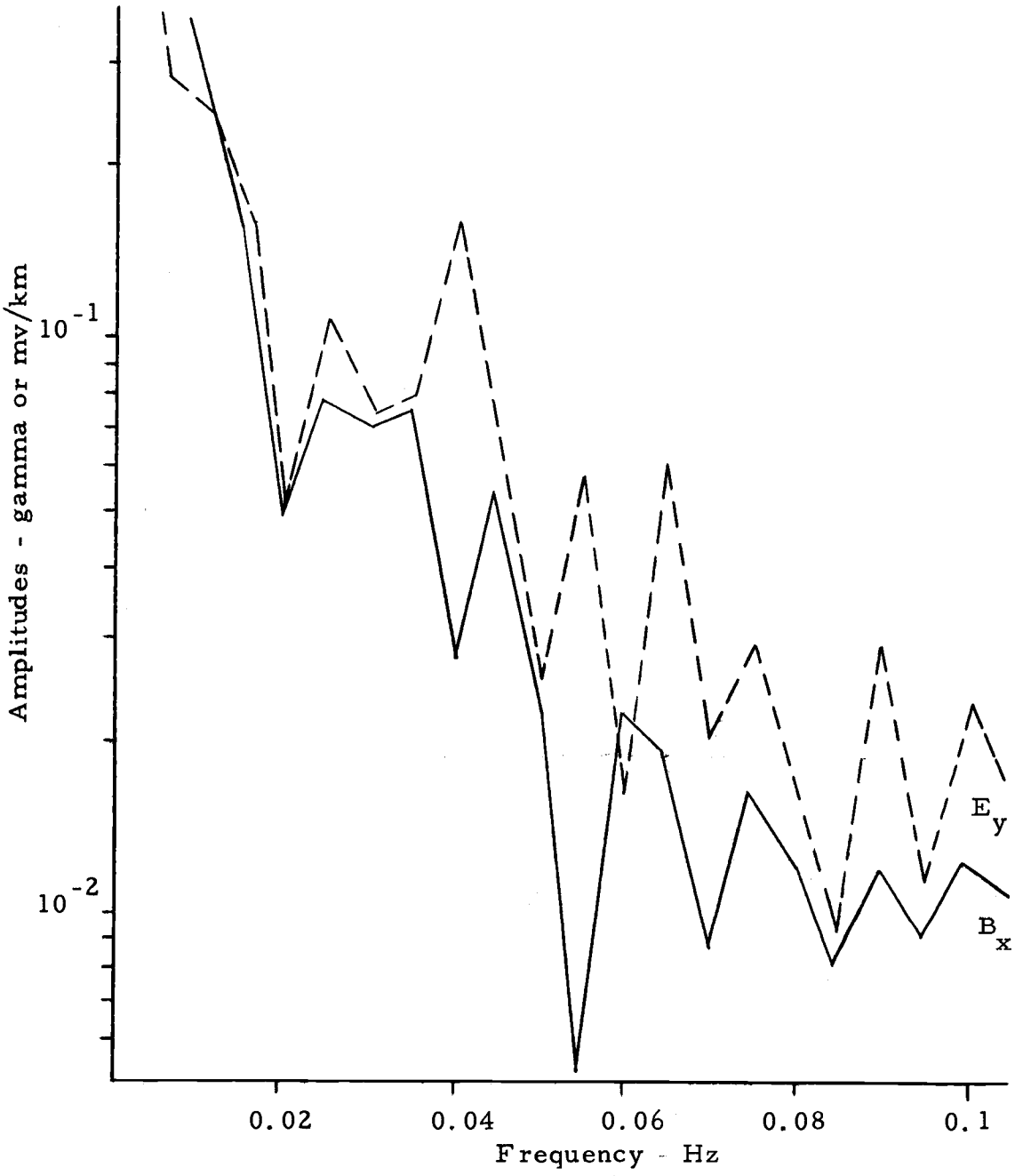

Figure 16. Fourier coefficients for station 11 (Poe Valley).

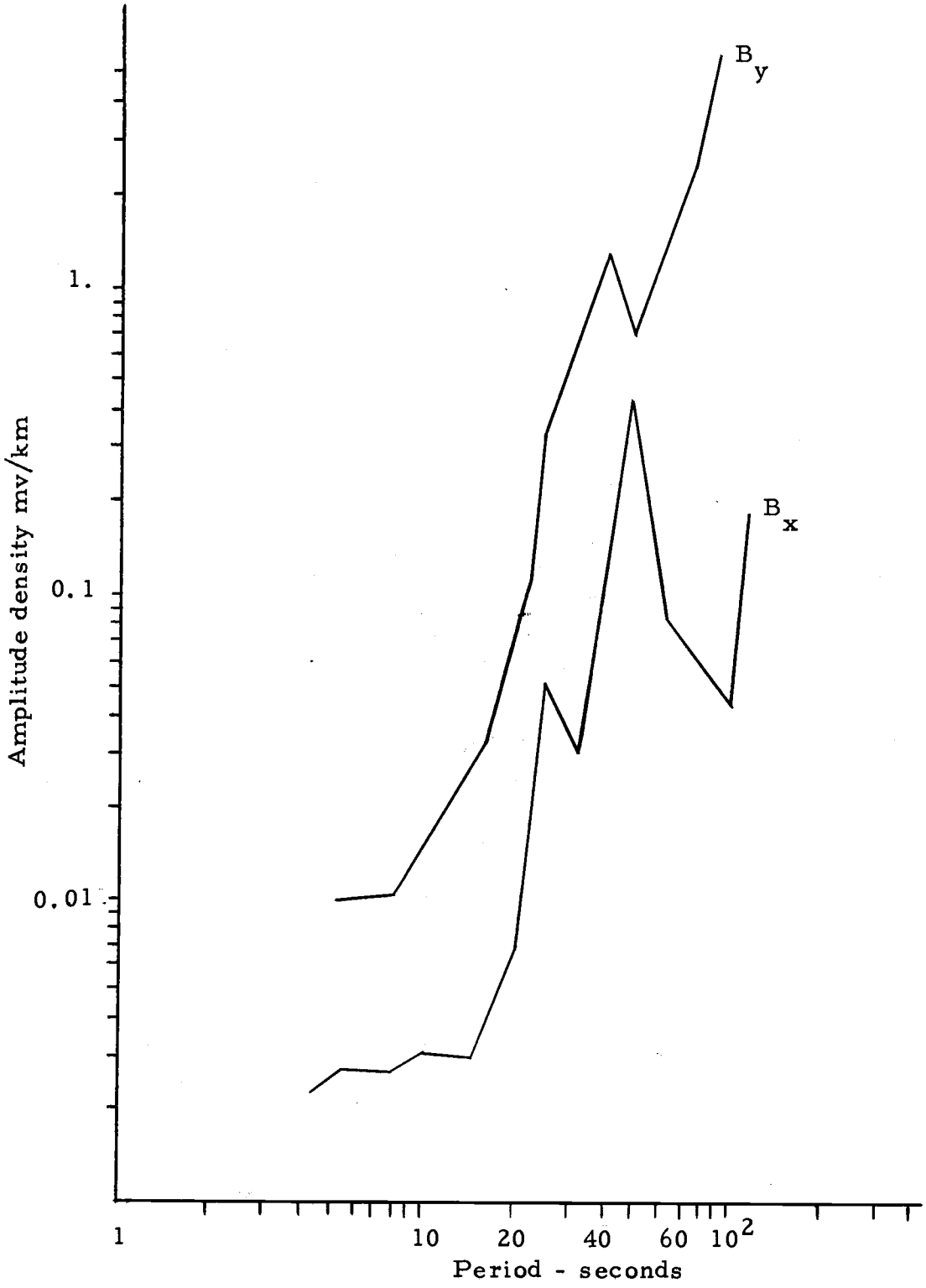

Figure 17. Power spectra for station 13 (South Klamath Hills).

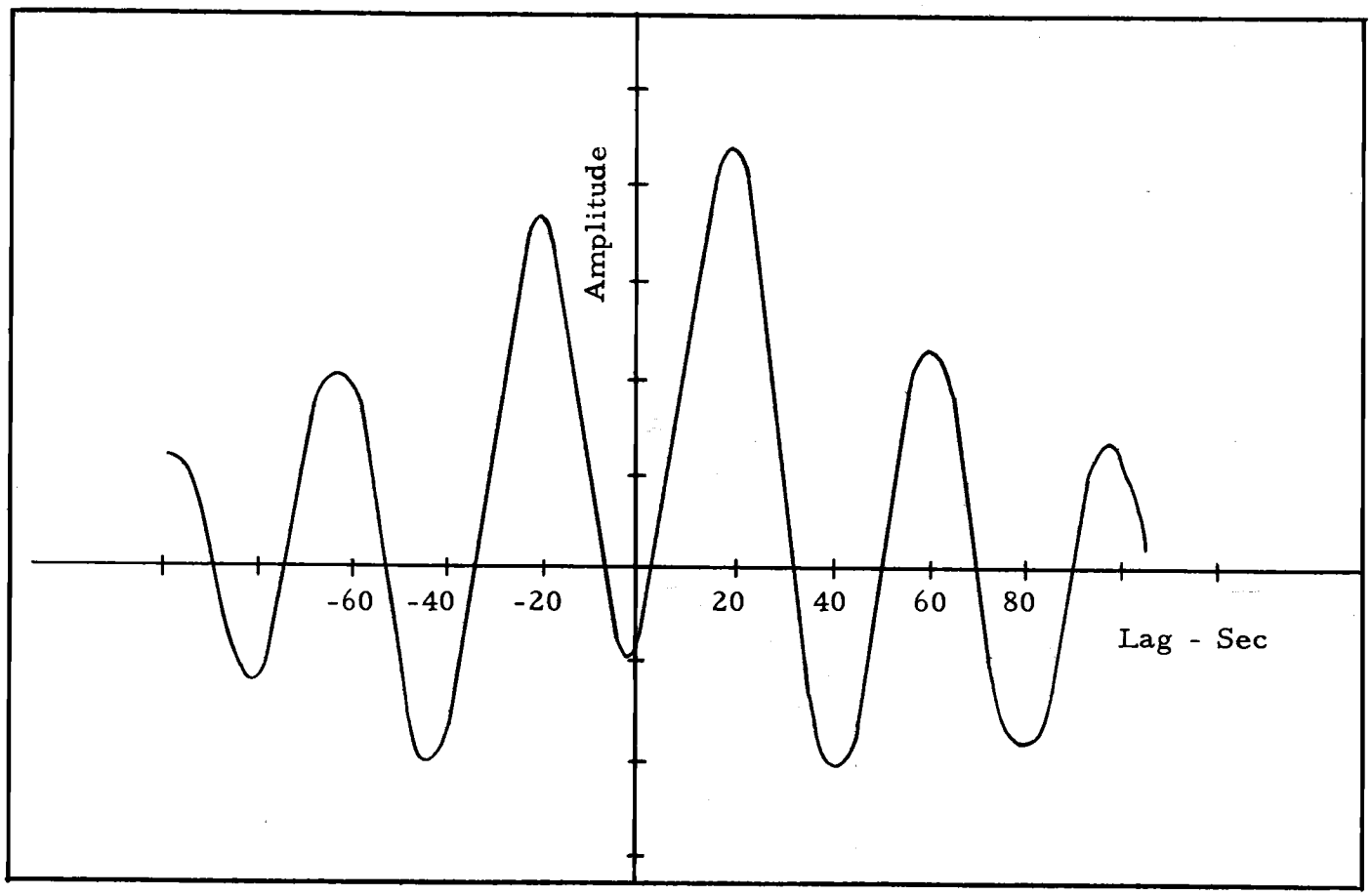

Figure 18. Cross correlation between B_x - E_y for station 13 (South Klamath Hills).

spectrum curves for other stations show characteristics similar.

Finally, the cross correlation for each pair of magneto-telluric components B_x-E_y and B_y-E_x was found by using the CROSS subroutine of *ARAND. In most cases analysed, the cross correlation was relatively poor. The cross correlation function for station 13 (South Klamath Hills) is shown in Figure 18. The figure shows that the magneto-telluric variations are highly sinusiodal in form and the dominant frequency is 0.05 Hertz.

Full description of the subroutines FOURTR, SPECTIC and CROSS may be found in the OS-3 *ARAND manual.

Individual Event Analysis

The low coherency between the magneto-telluric data pairs of E_x - B_y and E_y - B_x indicates that more direct interpretation methods be used rather than computer spectral analysis.

Examining all the available magneto-telluric records it was found that even with poor overall correlation, there exist particular events or groups of events with a good local magnetic-telluric correlation. The data from station 11 (Poe Valley) shown in Figure 15 provide a good example.

Although the overall correlation between the E_x and B_y records is not good, individual wave events with a satisfactory local correlation can be picked out and processed to determine impedance ratios

at various frequencies. It was therefore decided to use the individual event analysis rather than computer processing to derive impedance ratios over the range of periods involved. As an example of this procedure the following case will be described. The magneto-telluric records $B_x - E_y$ for station 7 (Lake Miller) are shown in Figure 19. This record extending over 400 seconds is typical of most of the present data. From left to right, the peaks that exhibit the best magnetic-telluric correlation includes 1, 3, 5, 9, 11, 13 and 26 which is not included in this figure. Using a procedure described by Birdichevsky (1959, 1965) and Keller and Frischknecht (1966), each peak can be separated into two parts, an ascending slope and descending slope from which two amplitudes and periods may be determined (Figure 19). The magnetic or telluric field amplitudes are taken as the amplitude interval between a peak and the nearest trough while the corresponding period is twice the time interval between these points. Wave impeadances over a range of periods can be derived in this way and the corresponding apparent resistivity may be found by using equation (53). The results for station 7 (Lake Miller) are listed in Table 3.

For convenience a scale factor has been introduced in the case of the data from the Lake Miller station shown in Figure 19. The scale factor shown applies to the predominant 25 second period. The data at this station show strong high frequency components that are

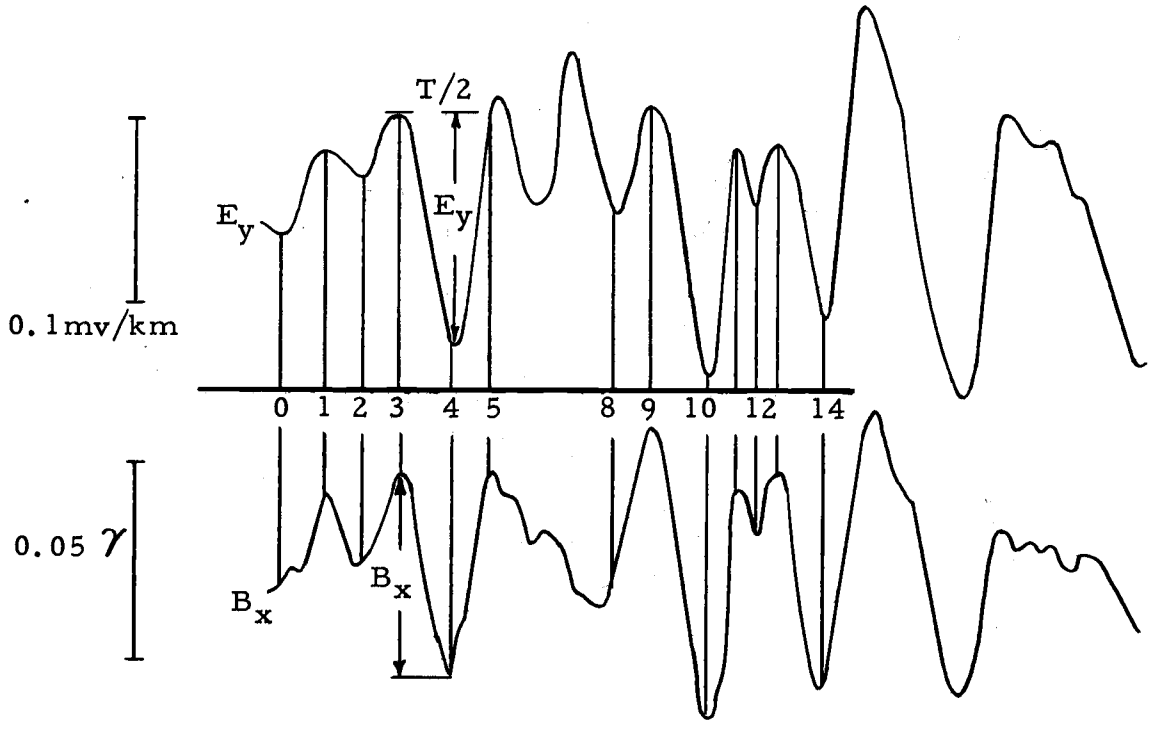

Figure 19. Magnetic-telluric records for station 7 (Lake Miller). displaying the procedure of deriving impedance ratios.

often absent from other magneto-telluric records. An example are the records for station 13 (South Klamath Hills) in Figure 14 which shows good correlation between sinusoidal activity of about 30 seconds period and little else at the shorter periods.

Table 3. Magnetic-telluric amplitudes and apparent resistivities for station 7 (Lake Miller) by individual event analysis.

Event number	B_x Gammas	E_y Mv/km	T Sec	Apparent resistivity Ohm-meters
1	.3	0.1	20	45
2	.03	.12	22	69
3	.017	.06	25	40
5	.04	.11	25	35
11	.025	.09	16	43
12	.02	.07	16	29
13	.05	.14	25	37
14	.06	.14	30	23
26	.09	.16	30	17
27	0.1	.18	28	20

Results of the individual event analysis of the present observational data are shown in Figure 20 to 24 where the magneto-telluric apparent resistivities are plotted against the corresponding periods. Resistivities have been obtained at a total of 17 stations. The series of stations 11 (Miess Lake), 7 (Lake Miller), 12 (Taluna), 13 (South Klamath Hills), 14 (Noble), 15 (Nuss Lake) and 16 Swan Lake)

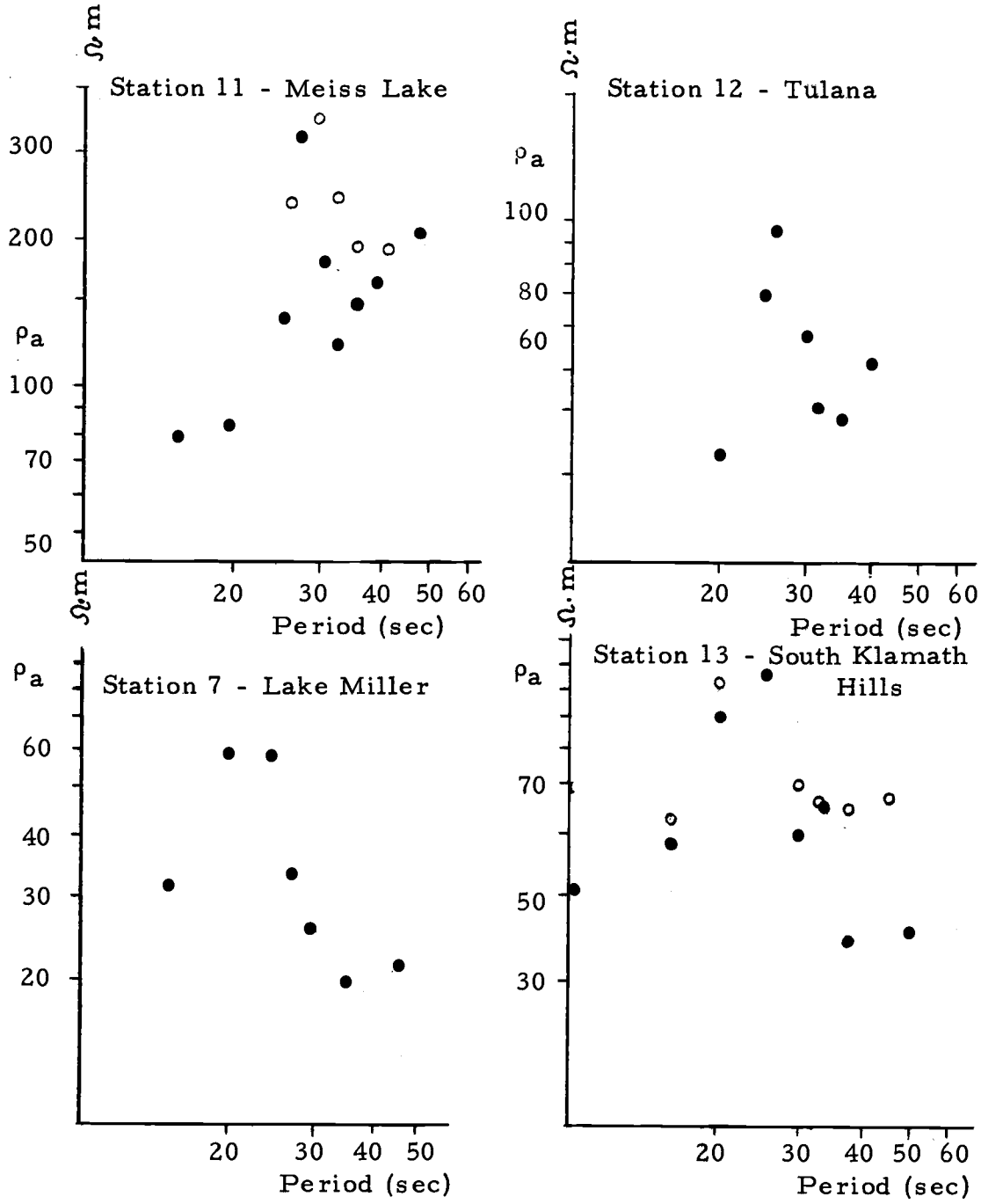

Figure 20. Apparent resistivities for stations 11, 12, 7 and 13. Solid circles represent north-south resistivities and hollow circles represent east-west resistivities.

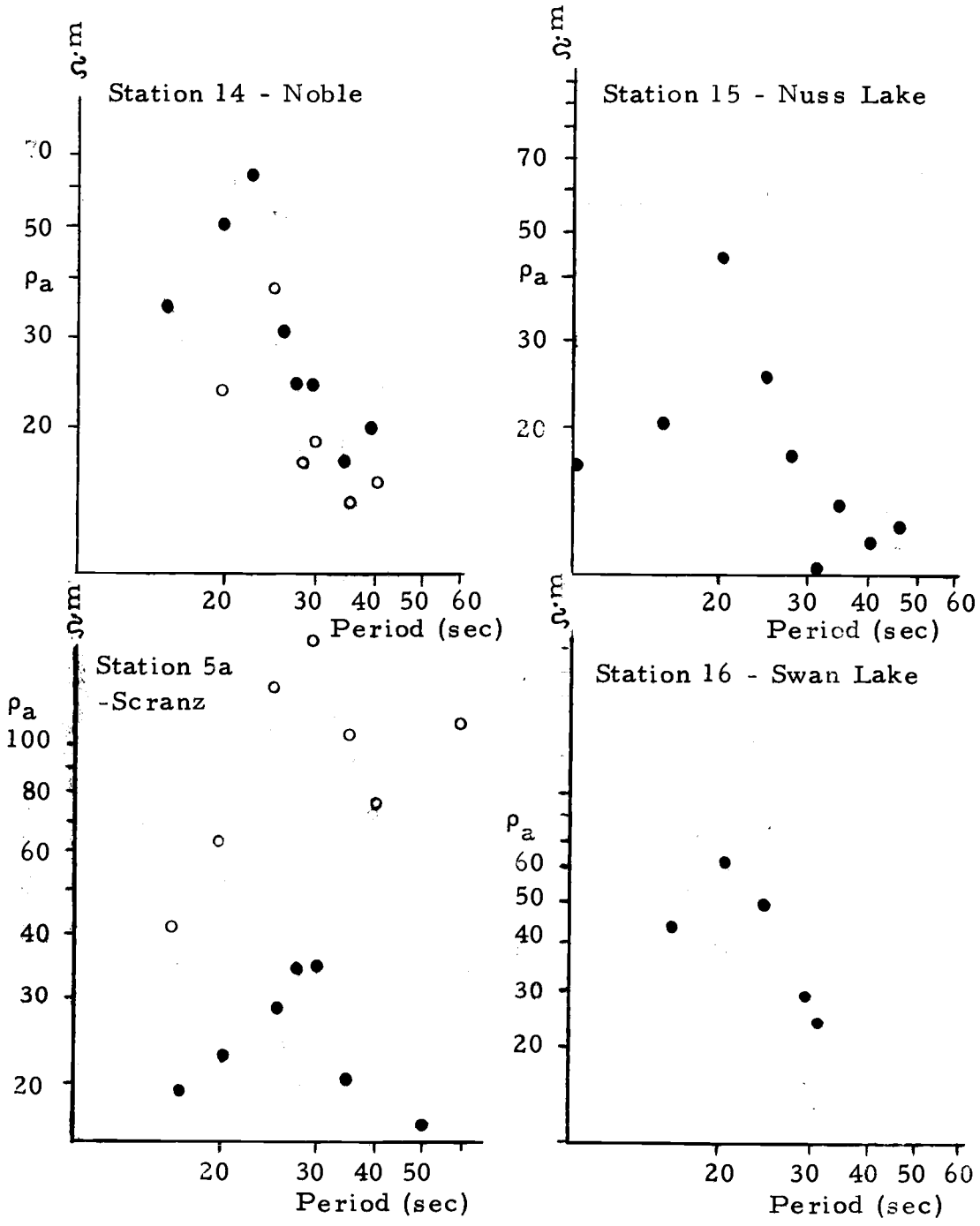

Figure 21. Apparent resistivities for stations 14, 15, 5a, and 16. Solid circles represent north-south resistivities and hollow circles represent east-west resistivities.

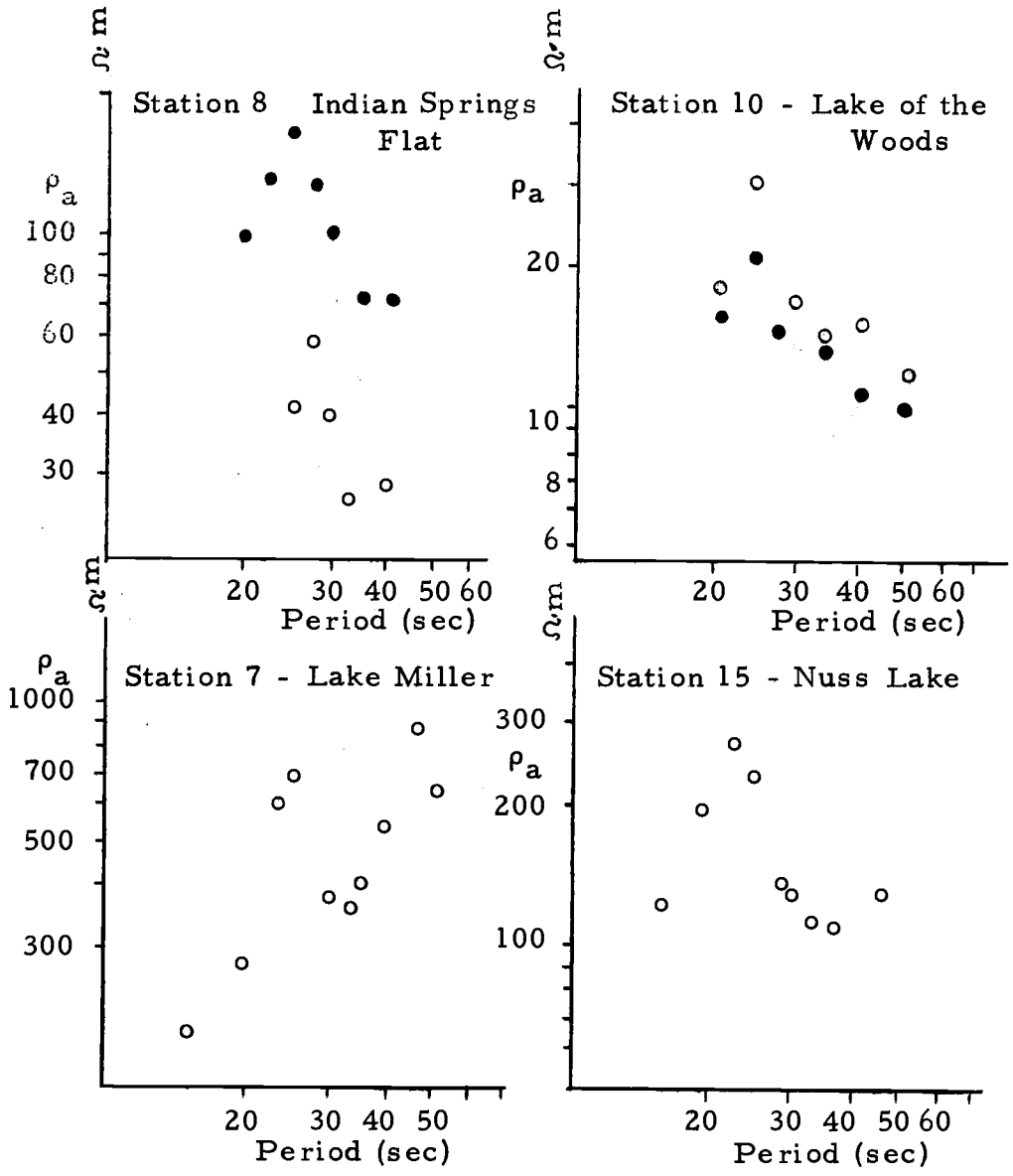

Figure 22. Apparent resistivities for stations 8, 10, 7 and 15. Solid circles represent north-south resistivities and hollow circles represent east-west resistivities.

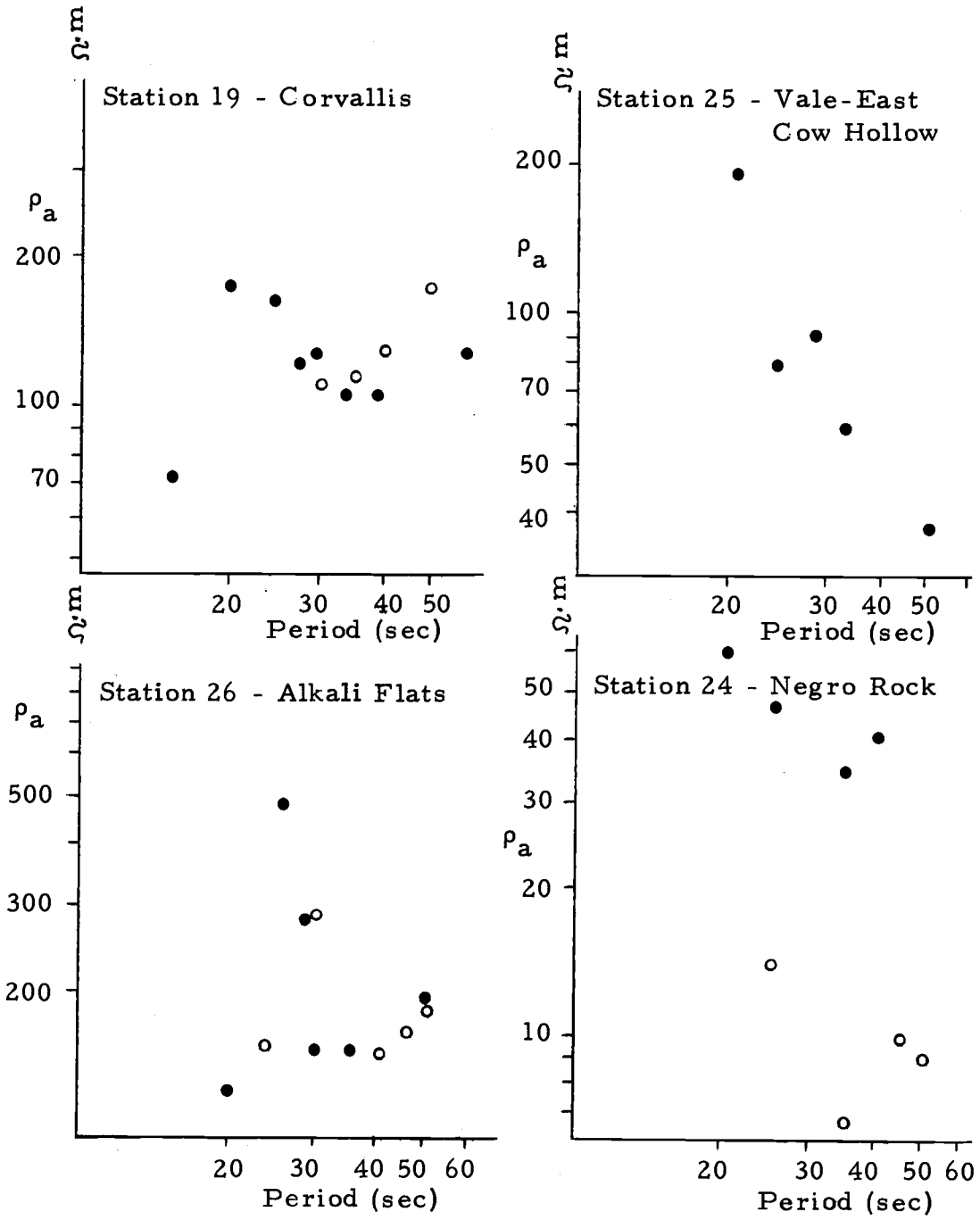

Figure 23. Apparent resistivities for stations 19, 24, 25 and 26. Solid circles represent the north-south resistivities and hollow circles represent east-west resitivities.

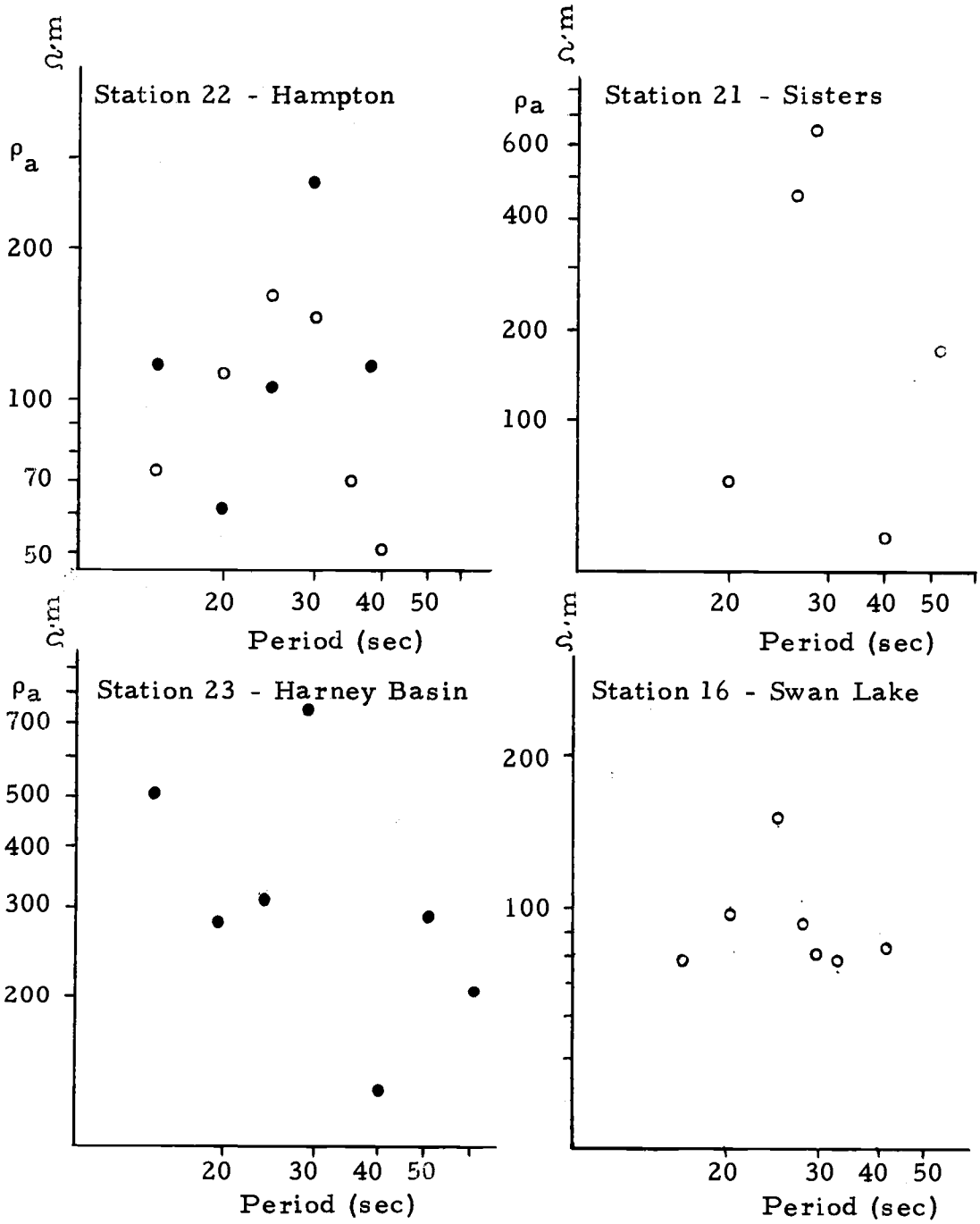

Figure 24. Apparent resistivities for stations 16, 21, 22 and 23. Solid circles represent north-south resistivities and hollow circles represent east-west resistivities.

transversing the Klamath Graben are of main importance. Station 19 is the Corvallis base station and stations 20 to 26 are located in Central and Eastern Oregon (see Figure 8).

In all these plots, the solid circles represent the north-south apparent resistivities obtained from the E_x/B_y impedance ratio. The hollow circles represent the east-west resistivities obtained from the E_y/B_x ratio.

The data points in almost all the plots indicate a greatly increased apparent resistivity in the 20 to 30 second period band. There appears to be a definite resistivity maximum in this band. A comparison with standard two or three layer magneto-telluric apparent resistivity curves (Yungul, 1961) shows that the slopes on both sides of the maximums are so steep that an impossible reflection coefficient is indicated. The maximums, therefore, appear to be anomalous. Since the anomaly is more or less consistent throughout the observed data, it is likely to be caused by a resonance phenomenon in the instrumentation which is not reflected in the calibration curves in Figure 10. Another, but less likely, possibility is that the individual event analysis procedure introduces a bias which enhances the impedance ratio in the 20 to 30 second period band. Obviously the anomaly is enhanced by the squaring of the impedance ratio in equation (53). It should be noted that a large scattering of the apparent resistivity values occur. This problem is magnified by the lack of values at higher and lower

periods. There are insufficient magneto-telluric signals outside the 20 to 50 second period band.

It is of interest to note that at stations in the Klamath Graben area, the east-west apparent resistivities usually appear to be larger than the north-south apparent resistivities.

INTERPRETATION

The presence of the anomalous maximums in the experimental apparent resistivity curves causes difficulties with regard to the application of standard curve matching methods in the interpretation of the observed data. We will, therefore, resort to other methods such as averaging and editing of the data by excluding more or less obvious anomalies.

Average Resistivities

In a first attempt to examine the data by smoothing out the resistivity anomalies, average resistivities over the whole range of periods were calculated for all sites. The data are listed in the following table. They appear to exhibit a fair degree of consistency. Some of the lower values appear to correlate with known geothermal manifestations.

The anomalous maximums in the apparent north-south resistivity plots all lie in the 20 to 25 second period band. The anomaly is quite narrow at most stations, including 12, 5a, 8, 14, 15, 7 and 26, and has a maximum of three to four times the minimum value that is usually found in the 30 to 35 second period band. At other stations such as 13 (South Klamath Hills), the maximum is broader or the period range is too narrow for a minimum value to be found.

Table 4. Average apparent resistivities for all available periods.

Station	Name	North-south resistivities	East-west resistivities	N-E Average resistivities
11	Miess Lake	205 ohm-meters	262 ohm-meters	233 ohm-meters
7	Lake Miller	39	421	230
12	Tulana	280	333	306
13	S. Klamath Hills	50	68	59
14	Noble	36	30	33
15	Nuss Lake	34	242	138
5A	Scranz	26	116	71
16	Swan Lake	7	131	69
10	Lake of the woods	13	19	14
8	Indian springs flat	103	35	69
19	Corvallis	128	134	131
21	Sisters	331	356	356
22	Hampton	136	134	135
23	Harney Basin	361		361
24	Vale-Negro Rock	44	9	26
25	Vale-E. Cow Hollow	67	331	199
26	Vale-Alkali Flats	221	173	197
Average		109	174	142

N - North-south
E - East-west

In the case of the east-west resistivities, the maximum exhibits the same characteristics except that they appear in the 25 to 30 second period band. The minima are found about the 35 seconds period and the resistivity values tend to rise from this point on. It is also noticed that the observed east-west resistivities have low values at periods less than 20 seconds.

The next step consisted in deriving the average resistivity values when the anomalous maximum is removed. We make the assumption that the maximum is narrow in range and is confined to the 20 to 30 seconds period band. The average resistivities are then found by considering only the end points of the resistivity plots.. The results are listed in Table 4. It is seen that the average values in this table are considerably lower than the average values over the whole range of periods that are listed in Table 4.

The north-south east-west average resistivity values given in the last column in Table 5 are plotted on a map of the Klamath Falls area in Figure 23. The data given are to be regarded as apparent resistivities for the upper 5 to 20 km of the local crust. The penetration depends upon the resistivity and is greater for higher values.

The data in Figure 25 are much too few to reveal a clear trend. Moreover, the very limited frequency ranges on which the data are based makes a more detailed analysis in terms of crustal layering very

Table 5. Average apparent resistivities after removing the data in the 20 to 30 seconds period band.

Station	Name	North-south resistivity	East-west resistivity	N-E Average resistivity
11	Miess Lake	188 ohm-meters	150 ohm-meters	169 ohm-meters
7	Lake Miller	21	330	175
12	Tulana	200	271	235
13	S. Klamath Hills	36	44	40
14	Noble	24	16	20
15	Nuss Lake	14	153	83
5A	Scranz	20	86	53
16	Swan Lake	4	80	42
10	Lake of the woods	11	15	13
8	Indian springs flat	50	30	40
19	Corvallis	103	134	118
21	Sisters		255	255
22	Hampton	100	79	89
23	Harney Basin	290		290
24	Vale-Negro Rock	35	7	21
25	Vale-E. Cow Hollow	67	277	172
26	Vale-Alkali Flats	140	146	143
Average		81	129	105

N - North-south
E - East-west

ambiguous. At this juncture, the following tentative conclusions can be arrived at.

1. The apparent resistivity data observed in the Klamath Falls area are low when compared to normal crustal values which in cases may be orders of magnitude larger. The data are therefore indicative of an enhanced electrical conductivity probably due to elevate subsurface temperatures in the region.
2. The resistivities decrease towards the northwest and north of the area.
3. When compared with available Wenner or Schlumberger D.C. resistivity data from well known high-temperature geothermal areas where values of the order of 1 to 10 ohm meter have been observed (Banwell et al., 1965) the data obtained in the Klamath Falls area are not indicative of typical high temperature conditions. However, the large scale average nature of the data is to be emphasized and this conclusion is tentative at best.
4. The apparent resistivities observed at station 25 and 26 in the Vale region shown in Figure 24 of the same order as the highest values observed in the Klamath Falls region. Station 24, on the other hand, displays quite low apparent

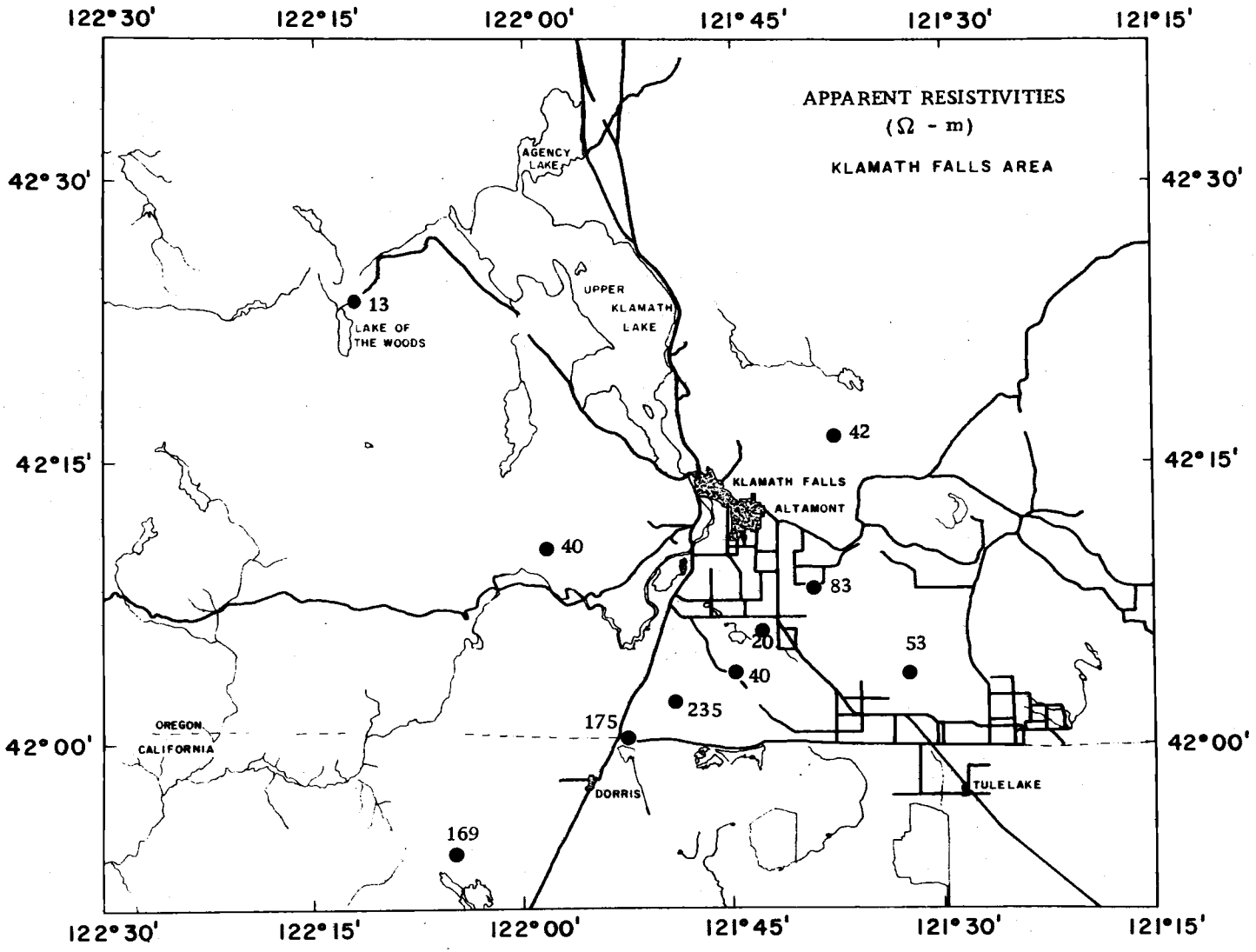

Figure 25. Average apparent resistivities for Klamath Falls.

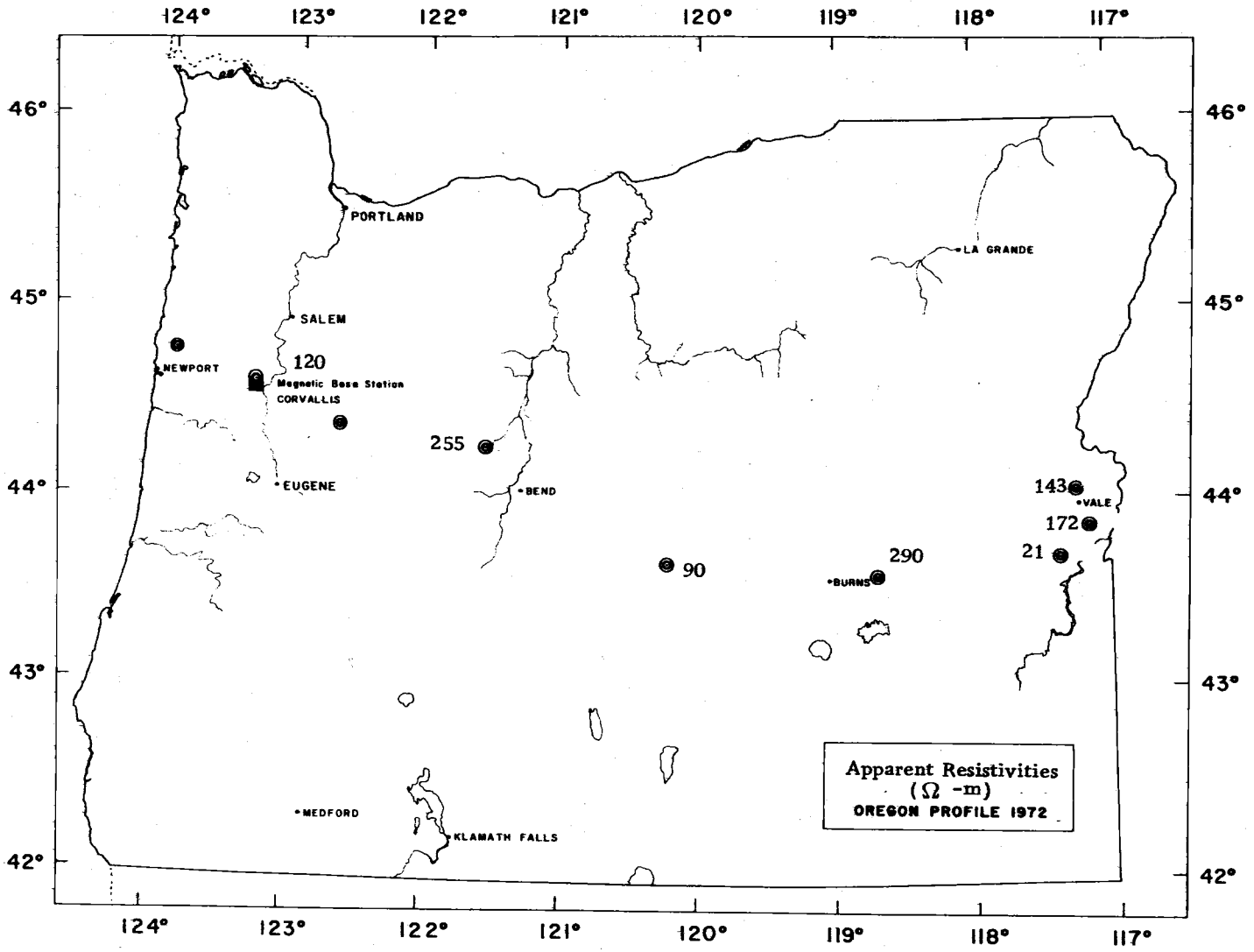

Figure 26. Average apparent resistivities for Central and Eastern Oregon.

resistivities which are probably caused by enhanced subsurface temperatures. The stations in Central Oregon have high apparent resistivities when compared with the data from Klamath Falls.

5. The range of the observed resistivity data and the correlation of low values with known surface geothermal manifestations indicate that magneto-telluric apparent resistivity data of the present type can be of considerable importance in the large scale reconnaissance type exploration for geothermal sources.

Interpretation in Terms of a Two-Layer Structure

The observation of the magneto telluric wave impedance at a single frequency furnishes one datum for the apparent average resistivity of the crustal section which is penetrated by the magnetic field at this particular frequency. Two impeadance values observed at two different frequencies can be applied to derive the parameters of a hypothetical two-layer model.

If the anomalous maximums are extracted from the data observed in the Klamath Falls region, two frequency bands remain in the data, that is, the 10 to 16 second and 30 to 40 second band. These two distinct bands can be used to derive a hypothetical two-layer structure on the basis of the two-layer formula (equation) given on page 32,

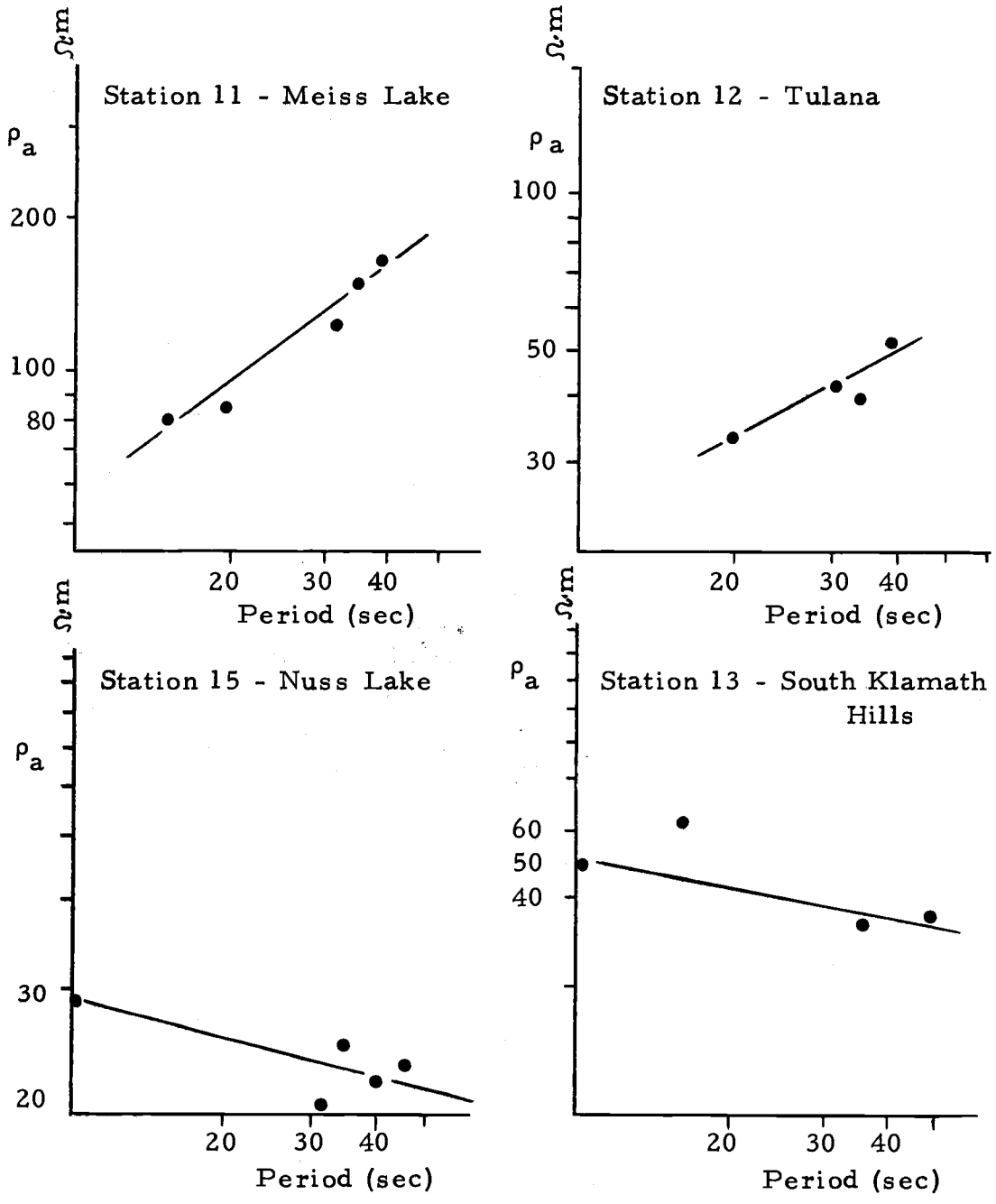

Figure 27. Interpolation lines between data points in the 10 to 20 and 30 to 40 second period band for stations 11, 12, 13 and 15.

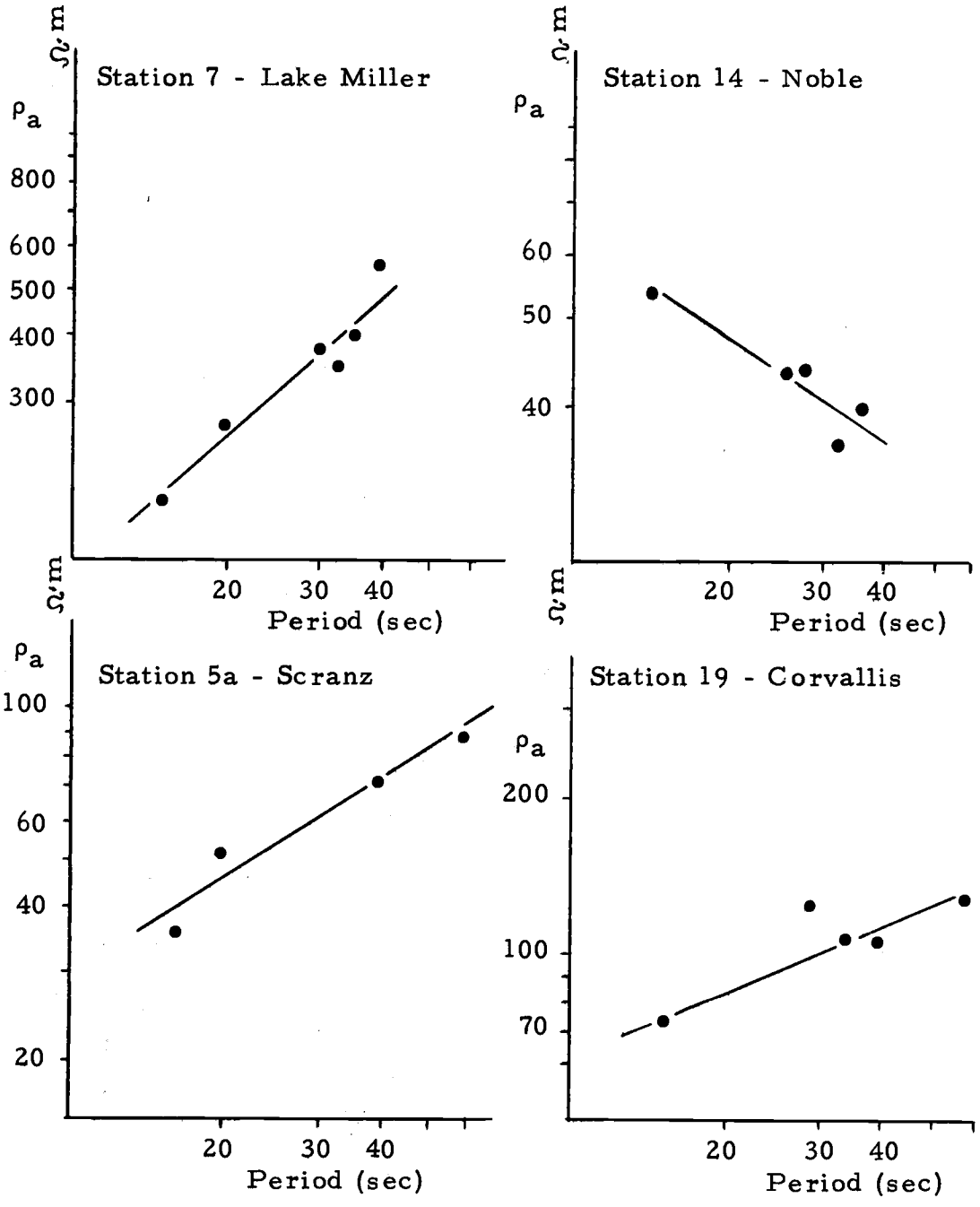

Figure 28. Interpolation lines between data points in the 10 to 20 and 30 to 40 second period band for stations 7, 5a, 14 and 19.

or, with the help of the standard two layer curves derived by Yungul (1961). The use of the standard curves require that the observational data obtained in the two end frequency bands be interpolated by a straight line which is then matched with a proper standard curve. In the present case this procedure has been applied to the data from eight stations in the Klamath Falls area. The relevant observational data and the interpolation lines are shown in Figures 25 and 26. The results are given in Table 6 below. The crustal sections obtained this way are shown in Figure 27.

As indicated in Figure 26, the two-layer interpretation reveals the rather remarkable result that the second layer resistivity is quite low below stations 13, 14 and 15 which are located close to the Klamath Falls geothermal area. The second layer resistivities are much higher for other stations. This appears consistent with the distribution of geothermal activity in the region. However, the tentative nature of the two-layer interpretation has to be underlined.

Table 6. Hypothetical two-layer interpretation based on the two end frequency bands.

Sites	Names	First layer resistivity	First layer thickness	Second layer resistivity	Direction
11	Miess Lake	80 ohm-m	13.3 km	4000 ohm-m	N
7	Lake Miller	160	16	16000	E
12	Tulana	140	16.7	2100	N
13	So. Klamath Hills	30	6.5	10	N
14	Noble	25	4	2	N
15	Nuss Lake	12	5	1	N
5A	Scranz	35	8.5	350	E
19	Corvallis	70	13	500	N

N - North-south E - East-west

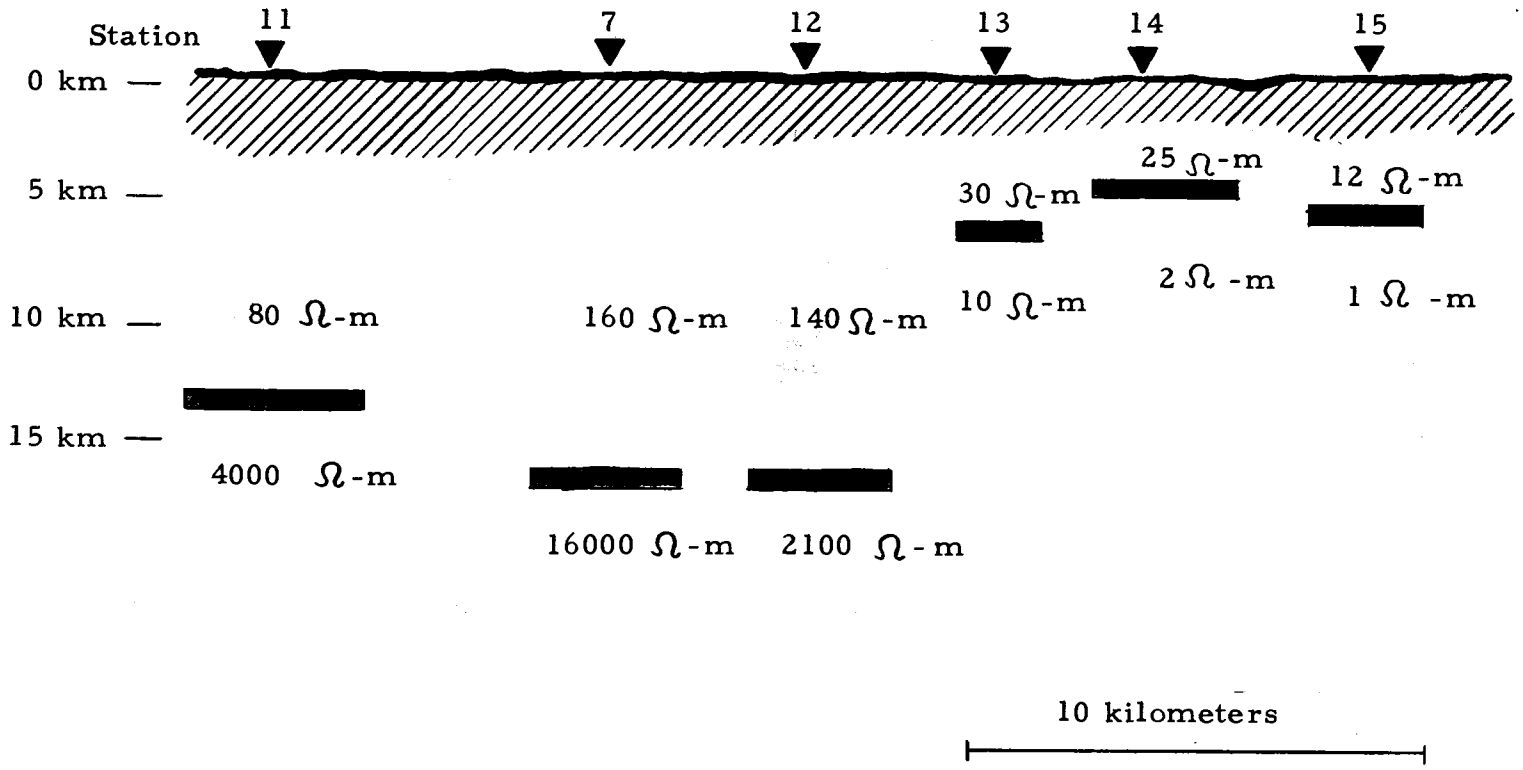

Figure 29. Hypothetical two-layer interpretation of observed data across the Klamath Graben from Table 5.

BIBLIOGRAPHY

Ballance, J., J. A. Baughman and L. Ochs 1973. OS-3 ARAND system: Documentation and Examples. Oregon State University Computer Center. CCR-71-01.

Banwell, C. J., and W. J. P. McDonald. 1965. Resistivity surveying in New Zealand thermal areas. Eighth Commonwealth Mining and Metall. Congr., Australia and New Zealand, New Zealand Section, paper no. 213, pp. 1-7.

Banwell, C. J. 1973. Geophysical Methods in Geothermal Exploration. UNESCO, Geothermal Energy (Earth Sciences, 12), pp. 41-48.

Berdichevsky, M. N. and B. E. Brunelli. 1959. Theoretical Premises of Magneto-telluric Profiling. Bull. (Izv.) Acad. Sci. USSR, Geophysics ser. no. 7, pp. 1061-1069.

Berdichevsky, M. N. 1960. Electrical Exploration with Telluric Currents, Quart. Colo. School of Mines, 60(1).

Bodvarsson, G. 1950. Geophysical Methods in the Prospecting of Hot Water in Iceland. J. Eng. Assoc. (Iceland), 35(5), pp. 49-59.

_____ 1961. Utilization of Geothermal Energy for Heating Purposes and/or Combined Schemes Involving Power Generation, Geating and/or By-Products. General Report GR/5, U.N. Confer. New Sources of Energy, Rome.

_____ 1969. Evaluation of Geothermal Prospects and the Objectives of Geothermal Exploration. Geoexploration, 8, pp. 7-17.

_____ 1971. The Exploration of Geothermal Resources in the Present and in the Future. UNESCO, unpublished.

Cagniard, L. 1953. Basic Theory of Magneto-telluric Method of Geophysical Prospecting, Geophysics, 18(3), pp. 605-635.

Chataev, D. N. 1960. The Determination of the Anisotropy Coefficient and the Angle of Inclination of a Homogeneous Anistropic Medium, by Measuring the Impeadance of the Natural EM Field. Bull. (Izv.) Acad. Sci. USSR, Geophysics ser. no. 4, pp. 617-619.

Combs, J. and L. J. P. Muffler. 1973. Exploration of Geothermal Resources. Geothermal Energy, ed. P. Kruger and C. Otte, Stanford University Press, Stanford, Calif., pp. 1-15.

Grant, F. S. and G. F. West. 1965. Interpretation Theory in Applied Geophysics. McGraw-Hill, New York, 583 pp.

Jacobs, J. A. 1971. Latitude-Dependent Characteristics of Long-Period Geomagnetic Micropulsation. JGR, 76(16). pp. 3675.

Keller G. V. and F. C. Frischknecht. 1966. Electrical Methods in Geophysical Prospecting. Pergamon Press, New York, 517 pp.

Keller, G. V. 1968. Electrical Prospecting for Oil. Quart. Colo. School of Mines, 63(2).

_____ 1970. Induction Methods in Prospecting for Hot Water. Geothermics, special issue 2, 2(1), pp. 318-332.

Koenig, J. B. 1973. Worldwide Status of Geothermal Resources Development. Geothermal Energy, ed. P. Kruger and C. Otte, Stanford University Press, Stanford, Calif., pp. 15-59.

Lee, W. H. K. and S. Uyeda. 1965. Review of Heat Flow Data. Terrestial Heat Flow, ed. W. H. K. Lee. Am. Geophys. Union, Monograph 8.

McNicol, R. W. E. and L. E. Johnson. 1964. Micropulsation Recording Equipment at Seattle. Boeing Sci. Res. Lab., Report 64-3, 34 pp.

Mechanics for Electronics. Model M24, Instruction Manual. Wilmington, Mass. 1973.

Microvoltmeter. Model A-60, Instruction Manual. Medistor Instrument Company, Seattle, Wash.

Moore, E. J. 1966. A Graphical Description of a New Method for Determining Equivalent NaCl Concentrations from Chemical Analysis. Trans. 7th Ann. Well Logging Symp., Prof. Well Log Analysts, Houston, Texas.

Peterson, N. V. and J. R. McIntyre. 1970. The Reconnaissance Geology and Mineral Resources of Eastern Klamath County and Western Lake County, Oregon. Oregon Dept. of Geol. and Min. Industries, Bull. 66, 70 pp.

Price, A. T. 1962. The Theory of Magnet-telluric Method When the Source Field is Considered. JGR, 67(5), pp. 1907-1918.

Rex, R. W. and D. J. Howell. 1973. Assessment of U. S. Geothermal Resources. Geothermal Energy, ed. P. Kruger and C. Otte, Stanford University Press, Stanford, Calif., pp. 59-69.

Sass, J. H. 1971. The Earth's Heat and Internal Temperatures. Understanding the Earth, ed. I. G. Gass, P. J. Smith and R. C. L. Wilson, Artemis Press, Sedgwick Park, England, pp. 81-87.

Sunde, E. D. 1949. Earth Conduction Effects in Transmission Systems. Van Nostrand, New York, 373 pp.

Tikhonov, A. V. 1950. Determination of the Electrical Characteristics of the Deep Strata of the Earth's Crust. Dokl. Akad. Nauk., 73, pp. 295-298.

Van Nostrand, R. G. and K. L. Cook. 1966. Interpretation of Resistivity Data. U. S. Geol. Survey Prof. Paper 499, Washington, D. C., U. S. Gov. Printing Office, 310 pp.

Vozoff, K. and R. M. Ellis. 1966. Magneto-telluric Measurements in North German Basin. Geophys. Prosp., 16, pp. 454.

Vozoff, K. 1972. The Magneto-telluric Method in the Exploration of Sedimentary Basins. Geophys. 37(1), pp. 98-141.

Wait, J. R. 1962. Theory of Magneto-telluric Fields. J. Res. N. B. S., 66D(5), pp. 509-541.

White, D. E., L. J. P. Muffler, and A. H. Truesdell. 1971. Vapor-dominated Hydrothermal Systems Compared with Hot-Water Systems. Econ. Geol., 66, pp. 75-99.

White, J. R. 1973. Characteristics of Geothermal Resources. Geothermal Energy, ed. P. Kruger and C. Otte, Stanford University Press, Stanford, Calif., pp. 69-95.

Yungul, S. H. 1961. Magneto-telluric Sounding Three-layer Interpretation Curves. Geophys. 26(4), pp. 465-473.